



**HAL**  
open science

## Interpenetrated biosurfactant-silk fibroin networks – a SANS study

Andrea Lassenberger, Anne Martel, Lionel Porcar, Niki Baccile

► **To cite this version:**

Andrea Lassenberger, Anne Martel, Lionel Porcar, Niki Baccile. Interpenetrated biosurfactant-silk fibroin networks – a SANS study. *Soft Matter*, 2021, 17 (8), pp.2302-2314. 10.1039/D0SM01869D . hal-03147255

**HAL Id: hal-03147255**

**<https://hal.science/hal-03147255v1>**

Submitted on 1 Mar 2021

**HAL** is a multi-disciplinary open access archive for the deposit and dissemination of scientific research documents, whether they are published or not. The documents may come from teaching and research institutions in France or abroad, or from public or private research centers.

L'archive ouverte pluridisciplinaire **HAL**, est destinée au dépôt et à la diffusion de documents scientifiques de niveau recherche, publiés ou non, émanant des établissements d'enseignement et de recherche français ou étrangers, des laboratoires publics ou privés.

# Interpenetrated biosurfactant–silk fibroin networks – A SANS study

Andrea Lassenberger,<sup>\*,1</sup> Anne Martel,<sup>1</sup> Lionel Porcar,<sup>1</sup> Niki Baccile,<sup>\*,2</sup>

<sup>1</sup>Institut Laue-Langevin, 71 Avenue des Martyrs, 38042 Grenoble Cedex 9, France

<sup>2</sup>Centre National de la Recherche Scientifique, Laboratoire de Chimie de la Matière Condensée de Paris, LCMCP, Sorbonne Université Paris F-75005, France

## Abstract

Silk fibroin (SF) based hydrogels have been exploited for years for their inherent biocompatibility and favorable mechanical properties which makes them interesting for biotechnology applications. In this study we investigate silk based composite hydrogels where pH-sensitive, anionic biosurfactant assemblies (sophorolipids SL-C18:1 and SL-C18:0), are employed to improve the present properties of SF. Results suggest that the presence of SL surfactant assemblies leads to faster gelling of SF by accelerating the refolding from random coil to  $\beta$ -sheet as shown by infrared and UV-visible spectroscopy. Small angle neutron scattering (SANS) including contrast matching studies show that SF and SL assemblies coexist in a fibrillary network that is, in the case of SL-C18:0, interpenetrating. The resulting overall network structure in composite gels is slightly more affected by SL-C18:1 than by SL-C18:0, whereas the structure of both SF and surfactant assemblies remains unchanged. No disassembly of SL surfactant structures is observed, which gives a new perspective on SF-surfactant interactions. The hydrophobic effect within SF is favored in presence of SL, leading to faster refolding of SF into  $\beta$ -sheet conformation. The presented composite gels, being an interpenetrating network of which one compound (SL-C18:0) can be tweaked by pH, open an interesting option towards improved workability and stimuli responsive mechanical properties of SF based hydrogels with possible applications in controlled cell culture and tissue engineering or drug delivery. The presented SANS analysis approach has the potential to be expanded to other protein-surfactant systems and composite hydrogels.

## Introduction

The fibrous protein silk fibroin (SF), produced by the *B. mori* silkworm has long been studied and used for biomedical applications for its exceptional mechanical properties, inherent biocompatibility and biodegradability.<sup>1,2</sup> SF consists of a hydrophobic heavy chain (FibH, ~390 kDa), and a light hydrophilic chain (FibL, ~26 kDa), held together by a disulfide bond. FibH comprises large repetitive units of alanine (ALA) and glycine (GLY) that fold into antiparallel  $\beta$ -sheet crystalline structures that are organized in an amorphous matrix to form a fishnet-like SF fibril.<sup>3</sup> Due to its unique primary structure, SF has the capability to form hydrogels with favorable mechanical properties, paired with biocompatibility and relative ease of fabrication. These hydrogels represent an ideal matrix for cell culture, tissue engineering and wound dressings and have therefore been investigated for centuries.<sup>4,5</sup>

For biomedical applications, SF is extracted from the cocoon of the silkworm in a degumming and dissolution process that includes boiling of the cocoons in sodium carbonate to remove the unwanted sericin coating. The fibers are then dissolved in highly concentrated chaotropic salt solutions such as LiBr and LiSCN, whereas Li<sup>+</sup> complexes with the carbonyl groups of SF, leading to a disassembly of SF secondary structure.<sup>6-8</sup> The obtained fibroin solution can then be regenerated into

various formats such as electrospun mats, hydrogels, sutures or even printable inks<sup>7, 9, 10, 11</sup> The regeneration and formation of SF hydrogels is governed by the spontaneous refolding of the ALA and GLY rich domains in FibH from random coil to  $\beta$ -sheet.<sup>12, 13</sup> In the present study, we use an adapted protocol for silk regeneration first introduced by Yamada *et al.*<sup>6</sup> and improved by Martel *et al.*<sup>14</sup> that leaves the FibH part of the protein intact and yields protein solutions with reproducible molecular weight distributions and gelling behavior.

Disadvantages of pure SF hydrogels are that the gelling is a rather slow and irreversible process and that the general workability of gels is moderate. Gelling times vary between days and weeks, depending on the preparation method, degumming history and gelling conditions. Researchers have improved the gelling properties by the addition of alcohols<sup>7</sup> and acids<sup>15</sup>, temperature change,<sup>16</sup> mechanical shear<sup>17-19</sup> polymers<sup>20</sup> or surfactants.<sup>7, 21, 22</sup> The mechanism behind accelerated gelling is generally attributed to the screening of charges within SF, whereas the carboxylic side chains of SF play the most important role: having an isoelectric point at pH 3.8-3.9<sup>23</sup> and thus an overall negative charge at neutral pH, protonation or neutralization of carboxylic groups occurs at acidic pH or upon addition of salts. Reduced hydrophilicity and repulsion between the chains are the consequence, favoring the hydrophobic effect and  $\beta$ -sheet formation and thus accelerated gelation.<sup>24</sup> A similar effect is observed for molecules that remove water from SF molecules, such as alcohols,<sup>25</sup> poly(ethylene)glycol,<sup>13</sup> and diverse anionic surfactants,<sup>22</sup> equally favoring the hydrophobic effect and leading to accelerated gelling.

More recently, researchers have shown that also natural surfactants, more precisely sophorolipids (SL), can act as gelators for SF.<sup>27, 28</sup> SL are a group of microbially produced biosurfactants with anti-microbial and anti-inflammatory properties.<sup>29, 30</sup> They are composed of a hydrophobic saturated (SL-C18:0) or mono-unsaturated (SL-C18:1) tail derived from stearic and oleic acid respectively, exposing a first hydrophilic headgroup, and a second hydrophilic headgroup composed of two bulky sugar moieties. Due to their unique amphiphilic structure, they assemble, depending on pH and saturation of the fatty acid chain, into micelles (SL-C18:1) or twisted ribbons (SL-C18:0).<sup>31</sup> SL-C18:0, when assembled into ribbons, forms a hydrogel itself that disassembles at basic pH. Whereas SL in micellar form have been pioneered by Dubey *et al.*<sup>27</sup> as gelators for SF, we are investigating the interaction of the more complex SL-C18:0 with SF in this study. Adding SL-C18:1 and SL-C18:0 to SF yields composite hydrogels that combine the properties of both compounds, whereas the reversible gelling of SL-C18:0 can be of particular interest since it opens a new path towards stimuli responsive tunable mechanical properties. Such composite gels that comprise the individual control of the properties of the single compounds have predominantly been pioneered for cell culture and tissue engineering applications. Control of the single compounds is achieved by UV and visible light,<sup>32</sup> chemical reactions<sup>33</sup> and pH<sup>7</sup> to alter the biochemical and mechanical properties of distinct parts of the gel. This allows for controlled delivery of bioactive molecules<sup>34</sup> and cell encapsulation for three-dimensional cell culture.<sup>35</sup> For SF-SL composite gels this could mean facilitated handling and control over hydrogel network density and mechanical properties by pH or enzymatic degradation to tune the response of seeded cells or the release kinetics of loaded drugs.

In this study we characterize the gelling kinetics of SF-SL composite gels, containing either SL-C18:1 or SL-C18:0, by UV-Vis absorption measurements. Attenuated total reflection infrared spectroscopy (ATR-FTIR) is used to determine the secondary structure of SF in the different gels and the structure of composite gels in their native state is investigated by small angle neutron scattering (SANS). We show, by simple subtraction of scattering intensities and contrast matching experiments, that SL micelles and ribbons coexist with SF, forming a fibrillary, and in the case of SL-C18:0, an interpenetrating network. Importantly, neither disassembly of SL structures nor specific SF-SL interactions are observed, which is controversial to the current opinion in literature on SF-surfactant interactions.<sup>21, 28</sup> We furthermore find, by means of model independent analysis of SANS data (generalized Guinier-Porod analysis and Kratky plots), that SL surfactant assemblies affect the final composite gel structure to slightly different extents, depending on their molecular structure. Our results and the applied analysis approach have the potential to be expanded to other protein-surfactant systems and composite hydrogels.

## Materials and Methods

**Materials.** *B. mori* cocoons were purchased from Cosrx, Korea; Sodium carbonate ( $\text{Na}_2\text{CO}_3$  anhydrous,  $\geq 99.5\%$ ), hydrochloric acid (HCl, ACS reagent, 37%), NaOH (BioXtra,  $\geq 98\%$ ) and iron (III) chloride ( $\text{FeCl}_3$ , 98% reagent grade), glycine ( $\geq 99\%$ ), coomassie blue G250, methanol ( $\text{CH}_3\text{OH}$ ,  $\geq 99.9\%$ ), acetic acid ( $\text{CH}_3\text{COOH}$ ,  $\geq 99\%$ ),  $\beta$ -mercaptoethanol ( $\text{HSCH}_2\text{CH}_2\text{OH}$ ,  $\geq 99\%$ ) and  $\text{D}_2\text{O}$  (99.9 atom %) from Sigma Aldrich, Lithium thiocyanate ( $\text{LiSCN} \times \text{H}_2\text{O}$ , crystalline) from Alfa Aesar, tris(hydroxymethyl)aminomethane (TRIS,  $\geq 99.8\%$ ), sodium dodecylsulfate (SDS, UltraPure™) from Thermo Fisher Scientific, Mini-Protean TGX Precast gels >any kD< and Precision Plus Protein all blue standard was purchased from BioRad, SpectraPor® Float-A-Lyzer dialysis tubes 100 kDa from Spectrum Labs, Sophorolipids SL-C18:1 (Sopholiance, batch no. 11103A, dry content  $60 \pm 6\%$ ) were purchased from Soliance, France. All chemicals were used as received without further purification. Milli-Q water (Millipore USA,  $R = 18.2 \text{ M}\Omega\text{cm}$ ) was used for all experiments.

**Silk fibroin (SF) extraction.** Silk fibroin was extracted with a modified method published earlier by Yamada *et al.*<sup>6</sup> and Martel *et al.*<sup>36</sup> Briefly, cocoons were cut into pieces and soaked in ice overnight. The pieces were peeled into thin layers and dried at  $22^\circ \text{C}$ . 5 g of peeled cocoons were degummed for 5 minutes in 2 L of 0.1% w/v  $\text{Na}_2\text{CO}_3$  at  $80^\circ \text{C}$  under vigorous stirring and subsequently rinsed with Milli-Q water. The degumming time of 5 minutes was found to be the ideal condition to ensure full removal of sericin and to prevent the degradation of fibroin. The degummed and dried fibers were dissolved at  $0.1 \text{ g mL}^{-1}$  in 20 M  $\text{LiSCN} \times \text{H}_2\text{O}$  overnight at  $24^\circ \text{C}$  under gentle stirring. Non-dissolved fibers and impurities were removed from the very viscous silk solution by centrifugation at  $20.800 \times g$  in portions of 1.5 mL. The obtained solution could be stored for months at  $4^\circ \text{C}$ .

For further processing into hydrogels, the solution was dialyzed for 1.5 days in a 100 kDa Float-A-Lyzer dialysis membrane against 1 L Milli-Q water without stirring and a minimum of five changes of water during 12 h in order to remove  $\text{LiSCN}$ . Removal of  $\text{LiSCN}$  was confirmed by colorimetric detection of the reaction of  $\text{SCN}^-$  with  $\text{Fe}^{3+}$ , which forms a dark red complex of penta aquathiocyanatoferrate(III). The pH of the SF solution after dialysis was 6.5 and all further experiments were carried out at this pH, where SF with an isoelectric point of 4 is negatively charged.<sup>37</sup> For SANS measurements all preparation steps starting from dissolution in  $\text{LiSCN}$  and including dialysis were done in  $\text{D}_2\text{O}$ ,  $\text{H}_2\text{O}:\text{D}_2\text{O}$  (49:51) and  $\text{H}_2\text{O}$ . The protein concentration was determined with a Thermo Fisher Nanodrop spectrometer by measuring the absorption at 280 nm taking the average of three individual samples that were measured three times each. For all further experiments the protein concentration was adjusted to  $7 \text{ mg mL}^{-1}$  ( $\cong 0.7 \text{ wt}\%$ ) with the desired solvent. SDS-PAGE was performed to verify the integrity of the protein. Gels were loaded with  $17 \mu\text{g}$  protein per well either in 1x TRIS sample buffer only or in 1x TRIS sample buffer containing 5%  $\beta$ -mercaptoethanol to cleave the disulfide bond between the heavy and the light chain of fibroin. A photo of the gels is provided in the supporting information (Figure S1).

**Sophorolipids (SL) synthesis.** Acidic sophorolipids (SL-C18:1) were prepared from a commercial batch of a sophorolipid mixture by alkaline hydrolysis which converts lactonic/acidic mixture into a fully acidic sophorolipid form. The method of extraction and purification has been described elsewhere,<sup>38</sup> a typical  $^1\text{H}$  solution NMR fingerprint is given in the reference. The compound used here is majorly (>80%) composed of the acidic SL-C18:1 cis form that forms micelles.<sup>39</sup> SL-C18:0 has been synthesized from SL-C18:1 by hydrogenation as described earlier.<sup>38</sup> Micellar solutions of SL-C18:1 were prepared by mixing the dried lipids at  $20 \text{ mg mL}^{-1}$  in  $\text{D}_2\text{O}$ ,  $\text{H}_2\text{O}:\text{D}_2\text{O}$  (49:51) and  $\text{H}_2\text{O}$  and adjusting the pH to 6.5 with NaOH or NaOD. Gels containing ribbons of SL-C18:0 were prepared as published earlier.<sup>31</sup> Briefly, 20 mg SL-C18:0 were dispersed in 1 mL solvent and brought to pH 11 with 1M NaOH or NaOD. The pH was then lowered very slowly with 0.5 M HCl or DCl under stirring and sonication to yield a hydrogel at pH 6.5. For all SF composite gels we used micellar solutions of SL-C18:1 and ribbon containing gels of SL:C18:0.

**Hydrogel formation.** To produce silk fibroin hydrogels, the silk solution was diluted to 7 mg mL<sup>-1</sup> by adding the desired amount of D<sub>2</sub>O or H<sub>2</sub>O and gentle homogenization by turning the vial up and down. Gelation was tested by turning the vial upside down and was considered to be completed as soon as all material stuck to the bottom of the vial (usually after ~3 weeks). For SANS measurements, SF solutions were filled directly into 1 mm quartz cuvettes for gelation and stored at 4 ° C.

Composite SF-SL hydrogels were prepared by adding the desired amount of a micellar dispersion of SL-C18:1 or ribbon containing gels of SL-C18:0 to a freshly prepared SF solution and turning it up and down gently for homogenization. All samples, including the controls were treated the same. For SANS measurements, the final concentrations of SF was set to 7 mg mL<sup>-1</sup> and that of both SL to 5 mg mL<sup>-1</sup>. We note that SL-C18:1 is present in micelles at 5 mgmL<sup>-1</sup> and SL-C18:0 as ribbons. The concentrations were chosen based on gelling kinetics experiments and with respect to suitable concentration ranges for SANS measurements. All gels were prepared in D<sub>2</sub>O, H<sub>2</sub>O:H<sub>2</sub>O (49:51) and H<sub>2</sub>O. Composite gels were named SF-SL-C18:1 and SF-SL-C18:0 respectively. SANS data were recorded four weeks after hydrogel formation when the gelling was considered to be completed. For UV-Vis absorption measurements with the plate reader, samples were prepared in covered 96 well plates as triplicates and stored at 4 ° C.

**Gelling reversibility.** To test the reversibility of gelling, 10 µL of 1M NaOH was added to pure SF gel and SF-SL-C18:0 (1 mL gel with a thickness of 0.5 cm) and allowed to penetrate into the gel for 12 h. The gels were inspected macroscopically for their fluidity by turning them upside down.

**UV-Vis Absorption measurements (optical density).** Following the gelation kinetics by means of absorption has been first suggested by Matsumoto et al.<sup>24</sup> Absorption of samples prepared in 96 well plates was measured on a BioRad microplate reader with Microplate manager 6 software at 490, 562 and 595 nm. SF concentrations of 1 to 10 mgmL<sup>-1</sup> and SL concentrations between 0.1 and 5 mgmL<sup>-1</sup> were investigated. Triplicates of each sample were prepared and measured over the course of 22 days. Absorption values were averaged and standard deviation calculated. The time point where absorption was constant for at least two days was considered to be the end-point of gelation for the respective sample. Gels for UV-Vis were prepared in H<sub>2</sub>O to exclude any effect of D<sub>2</sub>O on the gelling kinetics.

**Attenuated total reflection-infrared spectroscopy (ATR-IR).** IR spectra of the hydrogels were recorded on a Jasco 4600 FT/IR spectrometer with diamond single-reflection ATR equipment and a resolution of 4 cm<sup>-1</sup>, averaging 32 scans under N<sub>2</sub> atmosphere. Spectra were treated with the Jasco Spectra Manager™ Suite software and corrected by the atmospheric background and H<sub>2</sub>O. Gels for UV-Vis were prepared in H<sub>2</sub>O to avoid any effect of D<sub>2</sub>O on the secondary structure.

**Small angle neutron scattering (SANS).** SANS experiments were performed at the Institute Laue-Langevin in Grenoble, France on the instrument D11 at a neutron wavelength of 5.3 Å at three detector to sample distances (1.4, 8 and 39 m) to cover a  $q$ -range of  $0.001 \text{ \AA}^{-1} < q < 0.4 \text{ \AA}^{-1}$ , with  $q = \frac{4\pi}{\lambda} \sin\theta$ , where  $2\theta$  is the scattering angle between the incident and the scattered neutron beam. Acquisition time ranged from 1 min at large angles and 60 min at small angles. Boron carbide (B<sub>4</sub>C) was used as neutron absorber, measurement temperature was set to 25° C, 2D data was corrected for the electronic background and the empty cell and normalized to absolute scale using the transmission of the empty beam. Data were azimuthally averaged to yield the typical 1D intensity distribution  $I(q)$ . Data were reduced with the grasp software<sup>40</sup> provided at the beamline. Raw and reduced data are available at [doi:10.5291/ILL-DATA.9-13-778](https://doi.org/10.5291/ILL-DATA.9-13-778).<sup>41</sup>

**Fitting of SANS data.** Reduced data were treated for their respective background and fitted using the SasView software application<sup>42</sup> and Igor Pro software with NCNR SANS reduction macros.<sup>43</sup> Calculations for neutron scattering length densities are provided in the supporting information. Scale factors for all components were kept constant over the whole fitting process.

*Fitting of SF.* We chose a general shape-independent analysis approach with the advantage that no assumptions about the structure have to be done before fitting. Previous works employing SANS to characterize SF-SL hybrid networks have employed advanced model functions (e.g., pearl necklace) to fit the SANS profiles.<sup>44</sup> In the absence of specific proof

testifying the interaction between SF and SL, and considering the complexity of the SF-SL system, SANS data have been voluntarily treated with a model-independent approach, rather than using complex model functions.

The fitting approach is based on a generalized Guinier-Porod model developed by Hammouda<sup>45</sup> that has been introduced to fit SANS data from non-spherical objects such as rods and platelets. This model has previously been used to describe the acid-induced gelling of silk fibroin.<sup>8</sup> Here we combine the generalized Guinier-Porod model with a power law to account for the scattering from the gel structure at small angles ( $q < 0.0035 \text{ \AA}^{-1}$ ) which cannot be captured with the generalized Guinier-Porod model solely, giving the following term for the scattering intensity  $I(q)_{total}$ :

$$I(q)_{total} = I(q)_{power\ law} + I(q)_{Guinier-Porod} \quad (1)$$

where both terms are summed over the whole  $q$ -range. An example curve indicating the different  $q$ -regions is supplied in the supporting information (Figure S2). The power law accounts mostly at low  $q$  to the intensity, whereas the generalized Guinier-Porod model contributes to the scattering intensity mostly at mid and high  $q$ .

The scattering intensity  $I(q)_{power\ law}$  is defined as  $q^{-power}$  and  $I(q)_{Guinier-Porod}$  is given by the Guinier-Porod term

$$I(q)_{Guinier-Porod} = \begin{cases} \frac{G}{q^s} \cdot \exp\left(\frac{-q^2 R_g^2}{3-s}\right) & \text{for } q_1 \leq q \leq q_2 \\ \frac{D}{q^a} & \text{for } q \geq q_2, \end{cases} \quad (2)$$

where  $q$  is the scattering vector,  $G$  and  $D$  are the Guinier and Porod scaling factors respectively,  $R_g$  is the radius of gyration,  $a$  the Porod exponent and  $q_1$  and  $q_2$  the characteristic length scales.  $3 - s$  is a dimensionality parameter whereas the parameter  $s$  is introduced to help fitting non-spherical objects, *i.e.*  $s = 0$  for spheres,  $s = 1$  for rods and  $s = 2$  for platelets. For further details we refer to the original text.<sup>45</sup>

*Fitting of sphorolipids.* SL-C18:1 micellar solutions were fitted with a model for a core-shell ellipsoid<sup>46</sup> as reported earlier.<sup>47</sup> SL-C18:0 is known to form a gel that is composed of twisted ribbons.<sup>31, 48</sup> No complete fitting of these structures has been reported in the literature so far, attempts have been made to fit the structures with a lamellar model<sup>38</sup> which did not take into account the contribution of the gel formed by SL-C18:0. We attempted to fit SANS data by this approach by using a lamellar Caillé model (Figure S3A) which gave non-satisfying results. We thus used an approach that assumes the twisted ribbons as elliptical cylinders as has been described for twisted ribbon model peptides.<sup>49</sup> The model for an elliptical cylinder<sup>50</sup> was combined with a power law to account for the scattering at low  $q$  stemming from the gel structure that is formed by SL-C18:0. Finally, the correlation peak at high  $q$ , which has been attributed to the intermolecular stacking of SL-C18:0 molecules within the ribbon<sup>38</sup> was fitted with a Gaussian peak to qualitatively identify the peak position and eventual changes thereof (see also Figure S3B).

*Fitting of composite gels.* The SANS profiles of composite hydrogels were fitted by adding the contributions of each individual compound whereas all models were summed over the whole  $q$ -range. This approximation is the best approach to extract qualitative structural information on such complex systems. SF-SL-C18:1 was fitted with a combination of a power law, a generalized Guinier-Porod term and a core-shell ellipsoid model. SF-SL-C18:0 was fitted with a power law, a generalized Guinier-Porod term, a second power law, an elliptical cylinder model and a Gaussian peak.

## Results and Discussion

### Gelling Kinetics and secondary structure of composite gels studied by absorption measurements and ATR-FTIR

**Gelling kinetics ('optical density').** To characterize the gelling time and determine the ideal concentration- and time frame for following experiments, turbidity measurements can be used to monitor the progress of SF gelling.<sup>24</sup> Absorption was measured at three different wavelengths (490, 562 and 595 nm, the available wavelengths of the plate reader) to rule out any specific absorption of one of the components. Absorptions were similar and no specific absorption was detected, analysis was thus carried out for absorption at 595 nm only. Composite hydrogels were prepared at the natural pH of SF after dialysis, pH 6.5, since it has been observed by us and others<sup>27</sup> that SL-C18:1 at its initial pH of 4.1 causes rapid aggregation and phase separation of SF.

Absorption measurements at  $\lambda_{595\text{ nm}}$  ('optical density') were carried out for both composite gels. SL-C18:1 is transparent in the examined concentration range of 0.1 to 10 mgmL<sup>-1</sup>, SL-C18:0 however, is turbid itself already at low concentrations (below 5 mgmL<sup>-1</sup>), with an absorption larger than 2, we thus refrain from further interpretation on gelling kinetics for composite gels with SL-C18:0. Data for these preparations are provided for completeness in the supporting information (Figure S 4A). We note that macroscopically the gelling of SF was accelerated in presence of SL-C18:0.

The time point where absorption measurements had been constant for at least two days was considered to be the endpoint of gelling. Thus SF and SF-SL-C18:1 (0.1-1 mgmL<sup>-1</sup>) were monitored over the course of 22 days and SF-SL-C18:1 (2-5 mgmL<sup>-1</sup>) for 15 days, shown in Figure 1A. Similar to observations by Dubey *et al.*,<sup>27</sup> we find that the addition of micellar SL-C18:1 accelerates the gelling process of SF significantly. As illustrated in Figure 1A, the degree of gelation at day seven with SL-C18:1 concentrations as low as 4 mgmL<sup>-1</sup> exceeds that of the SF control without SL by far. The mechanism behind this acceleration of gelling can at this point not be answered specifically but might be a synergistic effect of charges and hydration, promoting the hydrophobic effect within SF and leading to rapid gelling by refolding into  $\beta$ -sheet structures.<sup>24</sup> Such an effect has been reported earlier for other negatively charged surfactants and SF<sup>21, 51</sup> and will be discussed in detail later. Based on the results of absorption measurements and with respect to suitable protein concentrations for SANS measurements, the concentration of SF for further experiments was set to 7 mgmL<sup>-1</sup> and that of both SL-C18:1 and SL-C18:0 to 5 mgmL<sup>-1</sup>, where both lipids are known to be present in their micellar or ribbon containing form.

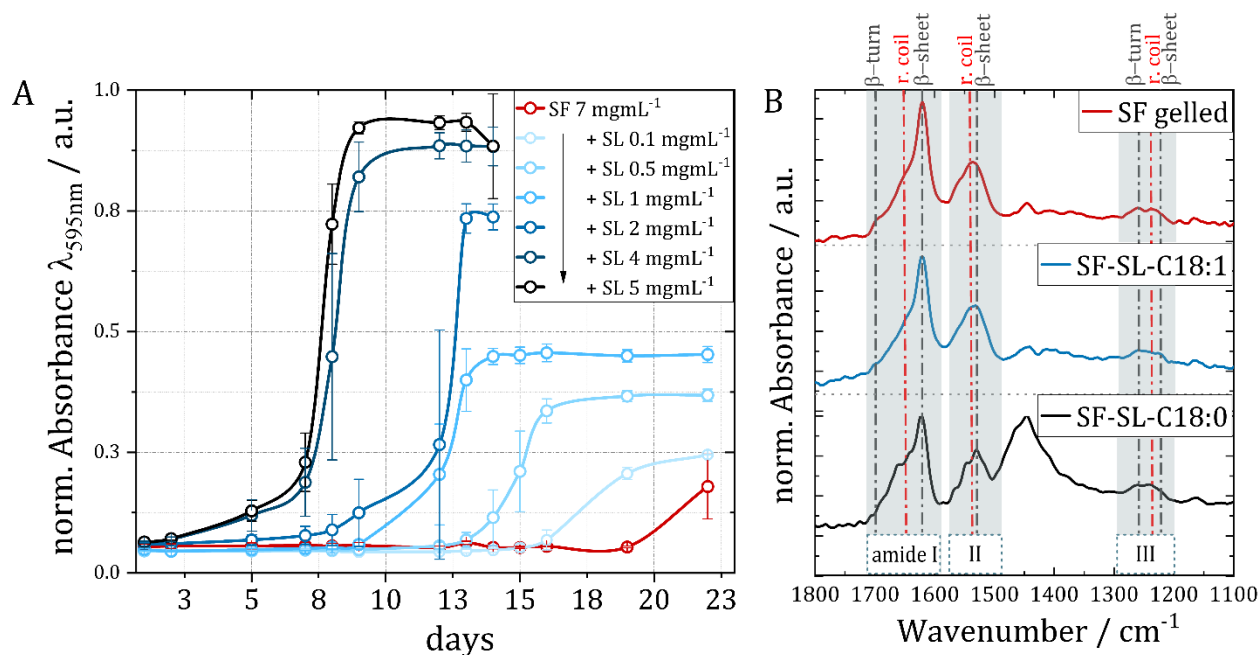


**Figure 1. A)** Absorption measurements at 595 nm to study the degree of gelling of SF (red) and SF-SL-C18:1 (blue) at 7 mgmL<sup>-1</sup> SF and different concentrations of SL-C18:1. Samples were prepared in triplicates and measured thrice each, the average values with standard deviation (error bars) are presented here. Gelling kinetics of SF-SL-C18:0 are not included here (see Figure S 4A) due to absorption values larger than 2. **B)** Normalized ATR-FTIR spectra of the amide I, II and III region of pure SF and composite gels confirming the conformational change from random coil (red vertical lines) to  $\beta$ -sheet and  $\beta$ -turn (grey vertical lines) upon gelling. Assignments from left to right: 1699, 1651, 1619, 1541, 1527, 1262, 1240, 1231 cm<sup>-1</sup>, details on assignments are discussed in the main text.

**Secondary structure (ATR-FTIR).** Gelling in SF is known to involve a conformational change of the hydrophobic amino acid sequences from random coil to  $\beta$ -sheet.<sup>24</sup> To verify that the accelerated gelling by sophorolipids also include this conformational change, we measured ATR-FTIR spectra of pure SF gels and the composite gels SF-SL-C18:1 and SF-SL-C18:0 (Figure 1B). Molecular vibrations in the amide I, II and III regions of proteins are known to correlate to their secondary structure and have been used to qualitatively and quantitatively study the secondary structure of silk fibroin.<sup>24, 52, 53</sup> The amide I region is found between 1700-1600 cm<sup>-1</sup> and is caused by mostly C=O stretch vibrations of peptide linkages (80 %) but also to a small extent by in-plane NH bending (20 %),<sup>54, 55</sup> and is therefore sensitive to the secondary structure of the protein backbone. The amide II band between 1600-1500 cm<sup>-1</sup>, caused by in-plane NH bending and CN stretching vibration of the protein backbone can provide additional information on the protein secondary structure<sup>55</sup> whereas the amide III region between 1300-1200 cm<sup>-1</sup> is usually of relatively low intensity and is thus not as extensively used for secondary structure analysis. However, it has been described in detail by Cai and Singh for SF<sup>56</sup> and will be discussed here to support our findings.

We note that ATR-FTIR spectra were measured in H<sub>2</sub>O since D<sub>2</sub>O can influence the secondary structure of SF.<sup>57</sup> Freeze-drying would be an alternative to gain signal intensity but is also known to alter the secondary structure of proteins.<sup>58, 59</sup> Measuring in H<sub>2</sub>O captures the native state of the hydrogels but has the disadvantage of a strong absorption band of H<sub>2</sub>O, overlaying with the amide regions. For this reason, the amide I, II and III band are analyzed only qualitatively and not quantitatively. In the amide I region all three gels show the signature of  $\beta$ -sheets with the characteristic band at 1619 cm<sup>-1</sup>.<sup>53, 60</sup> The peak for  $\beta$ -turns (band at 1699 cm<sup>-1</sup>)<sup>60</sup> is slightly more pronounced in pure SF gels when compared to the composites, which is also reflected in the amide III region. We note that the amide I band of the SF-SL18:0 composite gel has a slightly different shape compared to the other gels due to partial overlay of the carboxylate vibration band of the lipid



SL-C18:0 between 1710-1620  $\text{cm}^{-1}$ . Further information on this, along with a comparison of the IR spectra of composite gels and the respective pure SL compound is provided in Figure S5 of the supporting information. The vibrational band of random coil at 1541 $\text{cm}^{-1}$ ,<sup>53, 60</sup> is diminished for all three gelled samples along with a shift to 1527  $\text{cm}^{-1}$  that can be assigned to  $\beta$ -sheets.<sup>24, 54</sup> In the amide III region, the random coil vibration<sup>56</sup> at 1240  $\text{cm}^{-1}$  is shifted upon gelling, even if not very pronounced, to 1231  $\text{cm}^{-1}$  which is attributed to  $\beta$ -sheet.<sup>56</sup> We conclude that SF is mostly present in  $\beta$ -sheet conformation in both the pure and the composite gels; the gelling in presence of SL thus goes along with a conformational change from random coil to  $\beta$ -sheet, in analogy to pure SF.

### SANS study of composite silk-sophorolipid hydrogels

**SF-SL-C18:1.** We first discuss the system SF-SL-C18:1 as a model system to gain insight about the influence of SL on the gelling and refolding of SF and on the final network structure. All data discussed in this section are measured in  $\text{D}_2\text{O}$ . We note that the influence of  $\text{D}_2\text{O}$  on the final structure of SF was checked and the influence of  $\text{D}_2\text{O}$  on the structure of SL-C18:1 has been investigated earlier and is negligible.<sup>47</sup>

Figure 2A shows the neutron scattering intensity profiles of gelled SF (red), SL-C18:1 in micellar solution (yellow) and the SF-SL-C18:1 composite gel (black). Comparing the scattering intensities at  $q > 0.015 \text{ \AA}^{-1}$  supposes that the signal of the composite SF-SL-C18:1 gel is an addition of that of its single components. Any signal for the formation of an additional structure, i.e. a synergistic structure as has been reported for other systems<sup>61</sup> would be revealed in the SANS pattern.

To extract information about the influence of SL-C18:1 micelles on the folding and shape of SF and on the network structure, the signal of SL-C18:1 is subtracted from that of the composite gel to yield  $I(q)_{\text{SF-SL-C18:1}} - I(q)_{\text{SL-C18:1}}$  (Figure 2B, grey). The resulting signal superimposes with that of pure SF (Figure 2B, red) at  $q > 0.015 \text{ \AA}^{-1}$  and differs below that  $q$ -value. The fitted parameters extracted from the combined power law – generalized Guinier-Porod model are listed in Table 1.

The scattering in the Porod region at high  $q$  ( $q > 0.03 \text{ \AA}^{-1}$ ) is described by  $I(q) \sim q^d$  with the Porod exponent  $d$  being related to the surface fractal dimension  $D_s$  by  $d = 6 - D_s$ .<sup>62, 63</sup> For pure SF,  $d$  is fitted with  $3.8 \pm 0.04$ , corresponding to a surface fractal dimension  $D_s = 2.2$ , which suggests a slight interface roughness<sup>45, 62</sup> that has been described earlier for SF gels.<sup>64</sup> We hypothesize that this roughness can be attributed to the interface formed between  $\beta$ -sheet domains and the amorphous random coil matrix, which do not exhibit a very sharp boundary. A similar observation has been described by Putra *et al.*<sup>63</sup> for the structural reorganization within Poly(vinyl alcohol) hydrogels that, similarly to SF, form crystallites distributed in an amorphous matrix. When SL-C18:1 is present, the Porod exponent is increased to  $4.2 \pm 0.1$ , indicating that the interface in the composite system is sharper as for pure SF, possibly due to more defined boundaries between  $\beta$ -sheet domains and the amorphous matrix. The Radius of gyration  $R_g$  extracted from the Guinier-Porod fit is  $28 \pm 0.2 \text{ \AA}$  both in pure SF gel and the composite gel, whereas the fit is slightly deviating for the composite gel at  $q \approx 0.15 \text{ \AA}^{-1}$ . This could, together with the steeper Porod slope, be an evidence for small structural changes at that scale. The size of  $28 \text{ \AA}$  is in agreement with sizes reported for regenerated SF in literature<sup>57, 65</sup> and can most likely be assigned to  $\beta$ -sheet domains that are well located in this size regime.<sup>66, 67</sup> Definite certainty could however only be given by measuring the crystal size with neutron or x-ray diffraction. We note that this is object of further investigations whereas in this present study we focus on the overall hydrogel structure.

The mid  $q$ -region ( $0.0035 \text{ \AA}^{-1} < q < 0.02 \text{ \AA}^{-1}$ ) holds information about the shape of scattering objects in the range of tens of nanometers. For both curves in Figure 2B the slope is fitted with  $1.3 \pm 0.01$ , which points towards the existence of rod-like objects with a diameter in the nanometer range and a length that is outside the measured SANS range. Such rod-like structures have already been discussed for regenerated SF preparations<sup>37, 68, 69</sup> and we suggest that these could be fibrils, in which the  $\beta$ -sheet domains are dispersed in an amorphous matrix, similar to fibrils in natural silk.<sup>70</sup>

Very prominent structural changes in Figure 2B are observed in the low  $q$ -region ( $q < 0.0035 \text{ \AA}^{-1}$ ), where the scattering intensity of SF is increased in presence of SL-C18:1. This  $q$ -region gives information on a larger length scale and an upturn in  $I(q)$  in that region generally signifies intermolecular interactions, inhomogeneities or aggregation.<sup>65, 71, 72</sup> For our system this could be the formation of a network consisting of the above mentioned fibrils.<sup>37</sup> The increase in slope from  $2.1 \pm 0.01$  for pure SF to  $2.8 \pm 0.02$  for SF in the composite gel points towards an increase in network density.<sup>72</sup> We note that the low  $q$  part of our data exhibits only the tail of this network feature and its precise dimensions (such as pore size) cannot be extracted.

The Kratky representation (Figure 2C) ( $I(q) \cdot q^2$  vs  $q$ ) provides a qualitative measure for the folding and compactness of proteins,<sup>73, 74</sup> with globular folded proteins displaying a symmetric, bell-shaped curve with a distinct maximum due to their  $q^{-4}$  behavior. Pure SF shows a slightly asymmetric shape due to partial unfolding that can be ascribed to the random coil part of the protein. When SL-C18:1 is present, one observes that the maximum is shifted to lower  $q$  and that  $I(q)$  is starting to dominate over  $q^2$  at low  $q$  so that the bell shape is incomplete and values are tending to increase at  $q \rightarrow 0$ , which is characteristic for a dense gel network formation.<sup>75</sup>

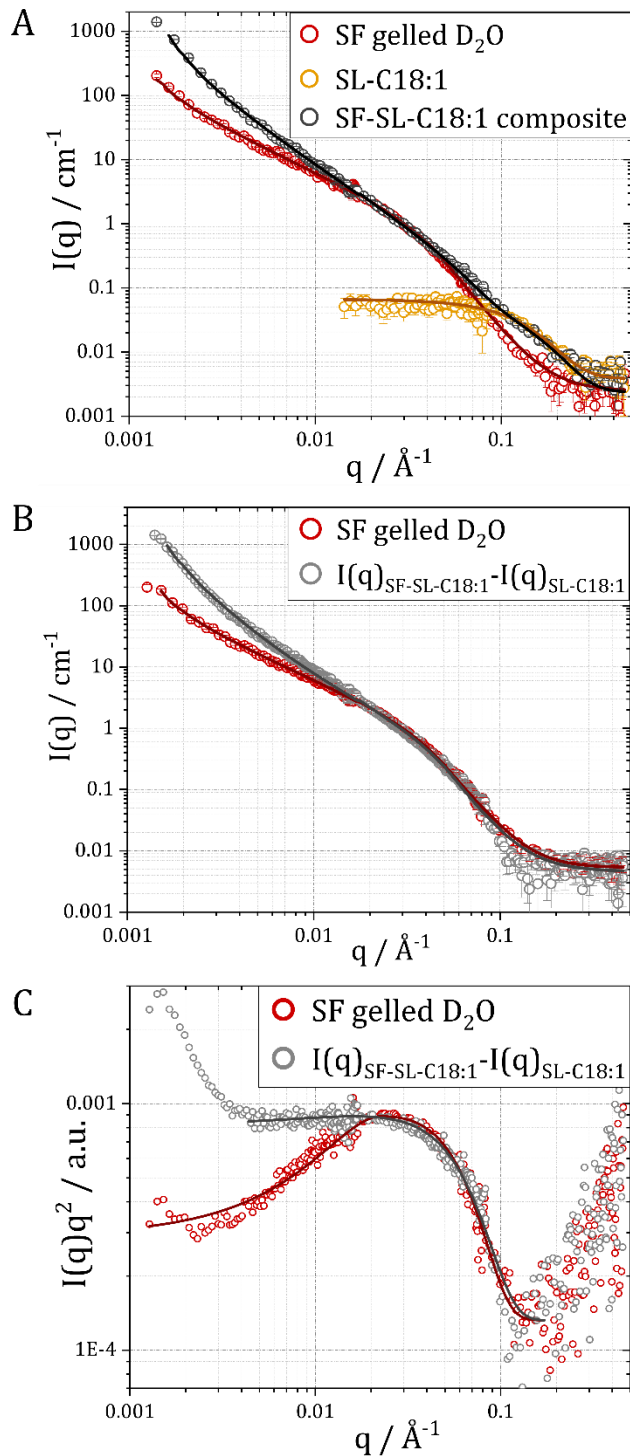


**Figure 2.** Neutron scattering data of hydrogels four weeks after dialysis, all in  $\text{D}_2\text{O}$  with SF at  $7 \text{ mgmL}^{-1}$  and SL at  $5 \text{ mgmL}^{-1}$ . **A)** Pure SF (red), pure SL-C18:1 (yellow) and SF-SL-C18:1 composite gel (black). **B)** The signal of SL-C18:1 was subtracted from the signal of the composite gel yielding the curve  $I(q)_{\text{SF-SL-C18:1}} - I(q)_{\text{SL-C18:1}}$  (grey), plotted together with the signal for pure SF (red). The curves overlap at  $q > 0.015 \text{ \AA}^{-1}$  with a small deviation at  $q = 0.15 \text{ \AA}$ , and differ significantly at low  $q$ , indicating that the addition of SL has an influence on the overall network structure in the nanometer range. Open symbols represent the experimental data, continuous lines the fitted data. **C)** Kratky plots in double log scale of pure SF (red) and the signal of SF in the composite gel after subtraction of SL-C18:1 ( $I(q)_{\text{SF-SL-C18:1}} - I(q)_{\text{SL-C18:1}}$ , grey).

**Table 1.** Fitted parameters for composite SF-SL hydrogels from a power law combined with a generalized Guinier-Porod model.  $I(q)_{SF-SL-C18:1} - I(q)_{SL-C18:1}$  and  $I(q)_{SF-SL-C18:0} - I(q)_{SL-C18:0}$  represent the fitted data for SF in the composite gel where the intensities of the respective SL are subtracted (*cf.* Figure 2B and Figure 4B, grey curves)

	$\chi^2$	$R_g / \text{\AA}$	power law $q < 0.003 \text{\AA}^{-1}$	slope $0.0035 < q < 0.02 \text{\AA}^{-1}$	Porod exponent
pure SF gel	1.4	$28 \pm 0.1$	$2.1 \pm 0.01$	$1.3 \pm 0.001$	$3.8 \pm 0.04$
$I(q)_{SF-SL-C18:1} - I(q)_{SL-C18:1}$	2.1	$28 \pm 0.2$	$2.8 \pm 0.02$	$1.3 \pm 0.01$	$4.2 \pm 0.1$
$I(q)_{SF-SL-C18:0} - I(q)_{SL-C18:0}$	1.4	$29 \pm 0.1$	$2.6 \pm 0.01$	$1.3 \pm 0.01$	$3.7 \pm 0.1$

The structural parameters determined for SF can now be used to fit the scattering profile of the composite gel (Figure 2A black) by combining it with the structural parameters of SL-C18:1 micelles.

SL-C18:1 in micellar solution is fitted with a model for a core-shell ellipsoid (Figure 2A, yellow) yielding dimensions of  $12 \times 41 \pm 0.3 \times 0.3 \text{\AA}$  and a shell of  $9 \pm 0.9 \text{\AA}$  which is in agreement with sizes reported earlier.<sup>47</sup>  $I(q)$  of the composite gel is fitted by combining a power law – generalized Guinier-Porod model for SF with a core-shell ellipsoid for SL-C18:1. Values for SF from  $I(q)_{SF-SL-C18:1} - I(q)_{SL-C18:1}$  and values of the ellipsoid fit for SL-C18:1 determined earlier are fed into the combined model for the composite gel; then the values for core and shell of SL-C18:1 micelles are allowed to vary. We find the dimensions of  $10 \times 41 \pm 0.2 \times 0.4 \text{\AA}$  core size and  $7 \pm 1.0 \text{\AA}$  shell thickness to be very similar to those of SL-C18:1 in the micellar solution, suggesting that SL micelles are not affected by SF, a result that is also supported by contrast matching experiments that will be discussed later. Alternatively, the signal of SF is subtracted from that of the composite gel to yield  $I(q)_{SF-SL-C18:1} - I(q)_{SF}$ , which recovers entirely the signal of the pure lipid (Figure S6A). Fitting with a core-shell ellipsoid gives a core size of  $10 \times 46 \pm 0.6 \times 1.0 \text{\AA}$  and shell thickness of  $8 \pm 0.4 \text{\AA}$  (Table S1), which is very close to the dimensions of pure SL-C18:1.

We summarize for SF-SL-C18:1 that the structure of both components is not or only slightly (sharper interface) affected at the nanoscale by the presence of the other compound. Structural changes are found at a larger length scale that concerns the network structure. In analogy to natural silk one can speculate that the assembly of  $\beta$ -sheet crystallites and the amorphous random coil matrix into fibrils form a denser network in presence of negatively charged SL micelles. A schematic representation of this interpretation is depicted in Figure 3.

The observed changes in network structure, in combination with the observed accelerated gelation and  $\beta$ -sheet formation are the result of a delicate interplay between hydration and electrostatic interactions<sup>20</sup> that are known to play an important role in protein folding<sup>76</sup> and in particular in the gelling of SF. The driving force for  $\beta$ -sheet formation in SF is generally accepted to be the hydrophobic effect in between large repetitive uncharged hydrophobic GAGAS units that build up over 86 % of the protein (as calculated from the protein sequence).<sup>77</sup> Why these hydrophobic interactions are favored and thus gelling is accelerated in presence of negatively charged SL-C18:1 micelles, cannot be answered specifically in this paper but synergetic effects cannot be ruled out. Faster gelling of SF has been observed in the presence of neutral, cationic or anionic surfactants,<sup>21, 22, 51</sup> including biosurfactants.<sup>27</sup> Whereas sodium dodecyl sulfate (SDS) and its interactions with proteins have long been studied, there is only little literature on the interaction of biosurfactants with proteins. Interestingly, SDS has been shown to induce fibrillation only below the critical micellation concentration (cmc), where free surfactant molecules interact with the hydrophobic domains of the protein,<sup>78</sup> whereas biosurfactants such as rhamnolipids mediate

fibrillation also above their cmc,<sup>79</sup> which suggests a different underlying mechanism. In the case of SDS and SF, an accelerated gelling has been ascribed to non-specific entropy-driven interactions between the alkyl chain of the surfactant and hydrophobic regions of SF, leading to the formation of mixed surfactant-protein micelles that construct the later gel network.<sup>21</sup> This mechanism has later been adopted by Dubey *et al.* to describe a SF-SL system similar to ours:<sup>28, 44</sup> Dubey *et al.* investigated the influence of SL-C18:1 on the gelling of SF with SANS at, with respect to our system, high concentrations of SL (30 mgmL<sup>-1</sup>). The accelerated gelling was attributed to the disassembly of SL micelles and the integration of SL molecules into the hydrophobic domains of SF, resulting in unfolding of the SF chain and formation of bead-like mixed SF-SL assemblies. We note that their presented SANS data were limited in  $q$ -range (minimum at 0.015 Å<sup>-1</sup>) and the relatively featureless curves were fitted with a rather complicated bead-necklace model, which could give rise to overinterpretations. Our observations are in contrast to their interpretation: bead-necklace structures would clearly involve interactions between SF and SL-C18:1 and thus result in a convolution of SANS patterns and changes in the high  $q$  range, which can be excluded from our data, where the signal of SL-C18:1 micelles is entirely recovered when SF is subtracted from the composite gel. We acknowledge however that the relatively higher concentrations of SL used by Dubey *et al.* could have given rise to different SF-SL interactions, similarly as it is known for other surfactants<sup>79</sup> and that at earlier stages of gelling, different SF-SL interactions might be possible. It is noteworthy that Dubey *et al.* used a different method for SF regeneration, leading to broad  $M_w$  size distributions that have been shown to interact differently with surfactants.<sup>80</sup> Another effect that could be synergistic with the already present hydrophobic interactions within SF, is the dehydration of SF molecules by highly hydrated SL sugar headgroups.<sup>27</sup> There is a growing consensus on that protein denaturation or folding is connected to the hydration state of the macromolecule,<sup>81, 82</sup> an effect that has long been known as ‘salting out’ in protein purification by kosmotropic ions in solution, according to the widely-known Hofmeister series.<sup>83</sup> In analogy to this, a similar effect of ‘salting out’ has been described for diverse surfactant-SF systems, e.g. for poly(ethylene)oxide (PEO) - SF composite hydrogels,<sup>13</sup> and for non-ionic and anionic surfactants and SF.<sup>22</sup> However, the ‘salting out’ effect and the Hofmeister series are discussed for ions in solution and SL are in micellar form, hence proof of such a hypothesis will certainly demand more work.

In the following section we will investigate the more complex system SF-SL-C18:0 to test and support our hypothesis of biosurfactant molecules coexisting with SF.

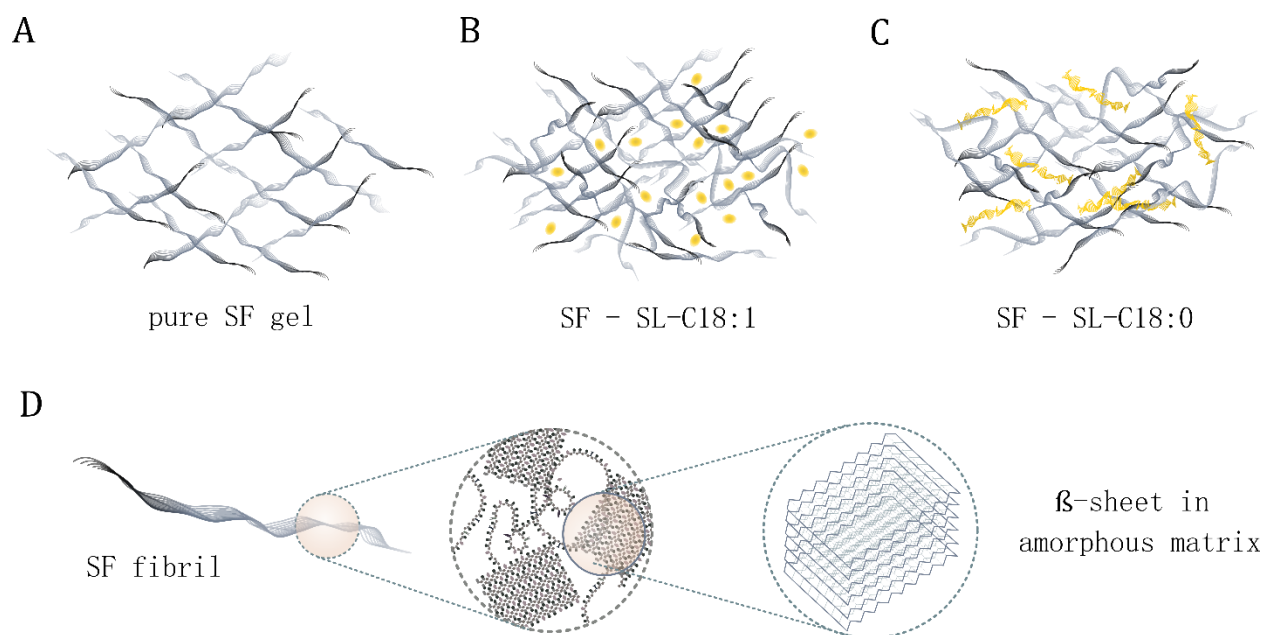


**Figure 3.** Schematic presentation of the discussed SF hydrogels. **A)** Pure SF is represented as entangled network of rod-like particles, presumably SF-fibrils. **B)** SF-SL-C18:1 composite gel with SL-C-18:1 micelles (yellow), coexisting with SF in a possibly denser network and **C)** SF-SL-C18:0 composite with SL-C18:0 twisted ribbons (yellow) and SF coexisting in an interpenetrated network. **D)** Proposed hierarchy in a silk fibril. We suggest, in analogy to natural silk, that silk fibrils constitute the observed rod-like particles, building up the whole SF network with  $\beta$ -sheet domains distributed in an amorphous random coil matrix in these fibrils.

**SF-SL-C18:0.** In an approach to create a hydrogel system with reversible properties, we prepared composite hydrogels of SF and SL-C18:0. SL-C18:0 has a fully saturated alkyl chain and forms, dependent on the pH, hydrogels itself. These hydrogels are composed of twisted ribbons and can be disassembled at basic pH.<sup>84</sup> Figure 4A shows neutron scattering intensity profiles for pure SF gels (dark red), SL-C18:0 (yellow) and for the composite gel SF-SL-C18:0 (black). SL-C18:0 has the typical scattering profile of twisted ribbons in agreement with what was reported earlier.<sup>38</sup> We recall that SL-C18:0 is fitted with a simplified model in this present study, assuming the ribbons to be elliptical cylinders, combined with a power law. The size of  $106 \times 244 \pm 0.6 \times 2.2 \text{ \AA}$  (minor axes diameters) extracted from the power law-elliptical cylinder fit is in good agreement with sizes reported earlier.<sup>38</sup> The characteristic peak at high  $q$  that identifies the repeating layer distance between the lipids within each ribbon,<sup>38, 85</sup> is fitted with a Gaussian peak at  $0.217 \pm 0.001 \text{ \AA}^{-1}$ , corresponding to a distance of  $29 \text{ \AA}$ , which is slightly larger compared to the  $27 \text{ \AA}$  reported by Cuvier *et al.*<sup>38</sup> We note that we solely use the position of the peak to identify eventual changes in the structure of SL-C18:0 when mixed with SF. We refer to Figure S3 in the supporting information for the complete fitting approach of SL-C18:0.

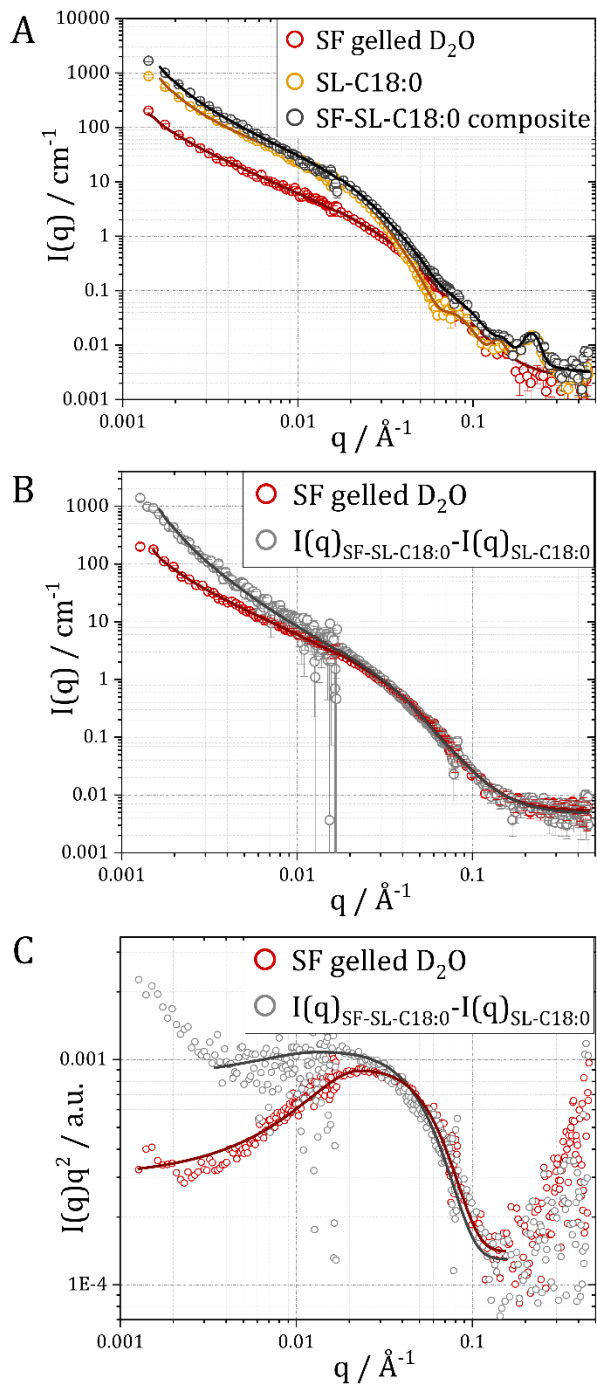


**Figure 4.** Neutron scattering data of hydrogels four weeks after dialysis, all in  $\text{D}_2\text{O}$  with SF at  $7 \text{ mgmL}^{-1}$  and SL at  $5 \text{ mgmL}^{-1}$ . **A)** pure SF gel (red), pure SL-C18:0 (yellow) and SF-SL-C18:0 composite gel (black). **B)** The signal of SL-C18:0 is subtracted from the signal of the composite gel, yielding the curve  $I(q)_{\text{SF-SL-C18:0}} - I(q)_{\text{SL-C18:0}}$  (grey), displayed with the signal for pure SF (red). **C)** Kratky plots of pure SF (red) and the signal of SF in the composite gel after subtraction of SL-C18:0 ( $I(q)_{\text{SF-SL-C18:0}} - I(q)_{\text{SL-C18:0}}$ , grey). Open symbols represent the experimental data, continuous lines the fitted data.

Figure 4A shows the neutron scattering intensity profiles of gelled SF (red), SL-C18:0 (yellow) and the SF-SL-C18:0 composite gel (black). In analogy to SL-C18:1, one can suppose that  $I(q)$  of the composite gel is a superposition of the scattering intensities of the single compounds.

Similarly as described for SL-C18:1, the signal of SL-C18:0 is subtracted from that of the composite gel to yield  $I(q)_{SF-SL-C18:0} - I(q)_{SL-C18:0}$  (Figure 4B, grey) to extract information about the folding of SF in the composite gel. Again, the resulting signal superimposes with that of pure SF (Figure 4B, red) at  $q > 0.02 \text{ \AA}^{-1}$  and differs below that value. The fitted parameters extracted from the combined power law – generalized Guinier-Porod model are listed in Table 1. For this system, the Porod exponent  $d$  is fitted with  $3.7 \pm 0.1$  which is close to that of pure SF and in contrast to SL-C18:1 ( $d = 4.2 \pm 0.1$ ). A surface fractal dimension  $D_s$  of 2.3 indicates that the interface roughness, i.e. the interface between  $\beta$ -sheet domains and the amorphous matrix, has not changed in presence of SL-C18:0. The fitted  $R_g$  of  $29 \pm 0.1 \text{ \AA}$  is close to that of pure SF and that of SF in presence of SL-C18:1 ( $28 \pm 0.1 \text{ \AA}$  and  $28 \pm 0.2 \text{ \AA}$  respectively). The slope at  $0.0035 \text{ \AA}^{-1} < q < 0.015 \text{ \AA}^{-1}$  remains at  $1.3 \pm 0.01$  in the composite gel, suggesting that the scattering particles in this size range are elongated in shape. At low  $q$  ( $q < 0.0035 \text{ \AA}^{-1}$ ) we observe a steeper slope ( $2.6 \pm 0.01$  vs.  $2.1 \pm 0.01$  in pure SF), indicating, in analogy to SL-C18:1, changes in the network structure that are slightly less pronounced for SL-C18:0. The smaller influence of SL-C18:0 on the network structure and fractal dimension can be explained by its smaller surface-to-volume ratio and thus less hygroscopic sugar headgroups on the surface of the twisted ribbons, as well as their location in- and outside the ribbons,<sup>38</sup> which might lead to a relatively smaller dehydration effect when compared to SL-C18:1, where all the sugar groups are located at the surface of the micelles. Finally we cannot exclude effects stemming from the dynamics of the system: while SL-C18:0 is practically a solid ribbon, SL-C18:1 could be regarded as a more dynamic system with SL molecules going on and off the micelles.

In analogy to SL-C18:1 the intensity profile of the composite gel (Figure 4A, black) is fitted by combining the models of the individual compounds and by using the fitted values for SF from Table 1. Allowing the values for the minor radius and axis ratio of SL-C18:0 to vary results in a ribbon size of  $98 \times 244 \pm 0.2 \times 1.0 \text{ \AA}$  (exact fitting parameters can be found in Table S1). This is close to sizes of pure SL-C18:0 ( $106 \times 244 \pm 0.4 \times 1.0 \text{ \AA}$ ) considering the complexity of the model for this composite gel, and suggests, similarly as was observed for SL-C18:1, that the SL-C18:0 assemblies remain unchanged in presence of SF. It is noteworthy that this integrity of SL-C18:0 assemblies is also shown by the presence of the correlation peak at  $q = 0.217 \text{ \AA}^{-1}$ , fitted at the same position and intensity as for pure SL-C18:0. The inverse approach of signal subtraction  $I(q)_{SF-SL-C18:0} - I(q)_{SF}$  recovers the signal of the pure lipid (Figure S6B) and, in combination with contrast matching experiments that are discussed later, confirms the hypothesis that SL molecules do not disassemble in presence of SF. The twisted ribbons of SL-C18:0 and SF coexist as an interpenetrating network that is in principle composed of two individual hydrogels, that are, interestingly, macroscopically homogenous (Figure S4B and Figure 5A).

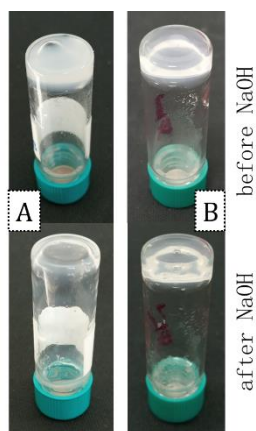




**Figure 5. A)** SF-SL-C18:0 composite gel before (top) and after addition of 10 $\mu$ L 1M NaOH and **B)** pure SF gel before (top) and after addition of NaOH (bottom). The composite gel was weakened by NaOH and a homogenous fluid was obtained whereas pure SF resulted in phase separation after addition of NaOH.

This coexistence of the gels is supported by observations upon changing the pH: the gelling of the SF-SL-C18:0 composite is reversible when the pH is changed from 6.5 to 11.3, yielding a macroscopically homogeneous fluid (Figure 5A), whereas the pure SF gel (Figure 5B) does not change. Since SL-C18:0 disassembles into negatively charged micelles and SF does not change at pH 11.3, the present results are rather interesting in that the obtained fluid is homogenous. We note that these experiments are preliminary and their analysis with SANS is ongoing, in order to resolve the structure of the disassembled hydrogel and to further investigate the mechanism of interaction between SF and SL.

**Contrast matching.** Contrast matching is an elegant method in neutron scattering that is applied to ‘mask’ one compound in a multi-component system by matching the contrast of the background with that of the compound. Here we aimed to measure the composite gels at the match point of SF (51 % D<sub>2</sub>O) to extract information about the structure of the lipids, to proof their integrity and the hypothesis that they do not disassemble when mixed with SF. The results of contrast matching experiments for SF-SL-C18:1 and a detailed discussion are presented in the supporting information (Figure S7) and are, due to low signal intensity, less explicit than the results for the system SF-SL-C18:0. In brief we can summarize that eventual structural changes of SL micelles (e.g. the formation of elongated micelles) are excluded and that there is no adsorption of SL-C18:1 on the SF network. The high scattering intensity at low  $q$  in the composite gel at the match point of SF is gone and the overall signal is comparable to that of the pure lipid at the SF match point.

In the following, contrast matching experiments for SF-SL-C18:0 are discussed. SF, SL-C18:0 and SF-SL-C18:0 composite gels were prepared at the match point of SF. The blue curve in Figure 6 shows that SF is well matched at the chosen conditions, the scattering at low  $q$  is negligible compared to the scattered intensities of the other samples. SL-C18:0 at the same condition (Figure 6, yellow) shows the typical profile of an elliptical cylinder as seen before in D<sub>2</sub>O. We note that the correlation peak at 0.217  $\text{\AA}^{-1}$  (*cf.* Figure 4A, yellow) is lost in the incoherent background. SL-C18:0 at contrast matching conditions is fitted with a combined power law - elliptical cylinder model, yielding a size of  $106 \times 232 \pm 0.6 \times 1.0 \text{\AA}$ , similar to the size fitted for pure SL-C:18:0 in D<sub>2</sub>O ( $106 \times 244 \pm 0.6 \times 2.2 \text{\AA}$ ). The scattering profile of the composite gel at SF - matching conditions (Figure 6, grey) almost superimposes with that of pure SL-C18:0 in matching conditions. Fitting with a combined power law - elliptical cylinder model yields a size of  $110 \times 238 \pm 0.4 \times 1.2 \text{\AA}$ , very similar to the size of pure SL in matching conditions, confirming that the ribbon structure of SL-C18:0 is contained in the composite hydrogel.

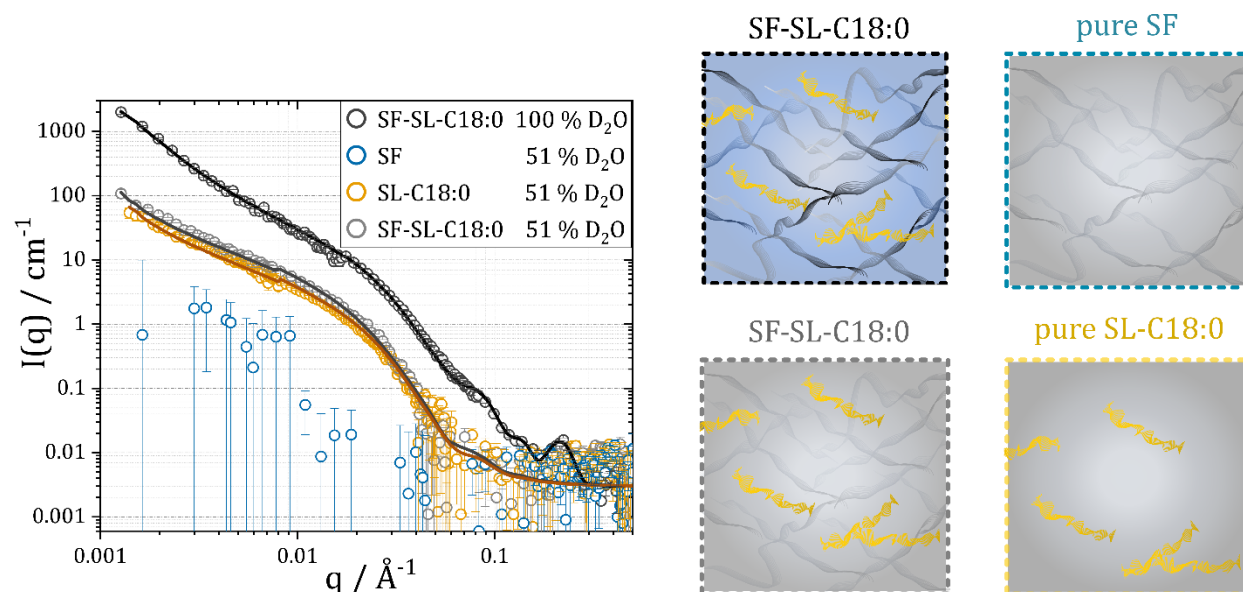


**Figure 6.** Scattering intensity profiles for hydrogels and lipids at SF-matching conditions and their respective schematic representation. Blue Background represents 100 % D<sub>2</sub>O and gray background 51 % D<sub>2</sub>O. **Pure SF** (blue symbols) is well matched at the chosen conditions and practically 'invisible'. **SL-C:18:0** (yellow) in matching conditions has the scattering pattern of an elliptical cylinder that superimposes with the signal of the **SF-SL-C18:0** composite gel (grey symbols), where SF is matched and the remaining signal is that of SL-C18:0. The scattering signal for **SF-SL-C18:0** composite gel (black) in D<sub>2</sub>O, where both components are visible, is plotted for comparison.

These results support our hypothesis discussed above under non-matching conditions, suggesting that SL structures do not disassemble and intercalate with SF as reported by other authors for anionic surfactants and SF.<sup>21, 44, 86</sup> We believe that these results can be transferred to and are true for SF-SL-C18:1 composite gels, since SANS results under non-contrast conditions suggest the integrity of SL micelles and their coexistence with SF. This however has yet to be proven under contrast matching conditions for higher concentrations of SL-C18:1. We also hesitate to name our hydrogel systems "orthogonal", since rheology measurements would be needed to fully prove the entire separation of the specific properties of each compound. Attempts were made to measure shear viscosity and shear modulus of the hydrogels and linking them to structural differences in the composite gels. However we could not find meaningful and reproducible values due to rapid aggregation and phase separation of the samples under shear and variabilities between different samples. We note that the literature on rheological properties of silk vary largely, dependent on sample preparation, concentration and the measurement method. As an example, shear viscosities for a 20 wt% solution of SF have been found to vary between 0.2 Pa.s and 28 Pa.s.<sup>87-89</sup>

## Conclusions

The influence of anionic biosurfactants, sophorolipids, on the structure and refolding of regenerated *B. mori* silk fibroin, and the structure of resulting composite hydrogels is investigated in a combined ATR-FTIR, UV-Vis and SANS study. The presence of both SL-C18:1 and SL-C18:0 leads to accelerated gelling of SF into  $\beta$ -sheet structures and to changes in the overall hydrogel network structure, as seen by SANS. These effects can be attributed to a depletion of water molecules by SL, favoring the hydrophobic effect within SF and thus  $\beta$ -sheet formation. The observed impact is slightly more pronounced for SL-C18:1 than for SL-C18:0, possibly due to the larger surface-to-volume ratio of SL-C18:1 micelles and a relatively larger number of hydrophilic groups exposed on the surface as compared to larger SL-C18:0 ribbons. Other types of hydrophobic interactions between surfactant molecules and SF at an earlier stage of gelling cannot be excluded but are

absent at the observed end state of gelling. We suggest that the structure of silk fibroin and sophorolipid composite hydrogels to be a fibrous network that is, in the case of SL-C18:0, interpenetrating. Importantly, SL structures do not disassemble and intercalate into SF domains, but SL-C18:1 negatively charged micelles and SL-C18:0 twisted ribbons coexist with SF, as is supported by SANS contrast matching methods. The SANS analysis approach and proposed alternative view on SF-SL interactions presented here can be expanded to other protein-surfactant and hydrogel systems to elucidate their structure. This will allow to eventually tailor their mechanical and structural properties, important for applications in cell culture and tissue engineering. In this context, the system SF and SL-C18:0 is due to the reversible gelling of SL-C18:0 of particular interest and object of further investigations, opening possibilities towards workable and stimuli-responsive SF based hydrogels.

### Conflicts of interest

There are no conflicts of interest to declare.

### Acknowledgements

This work received financing by FILL2030, a European Union funded project within the European Commission's Horizon 2020 Research and Innovation programme under grant agreement No 731096. Traveling related to this work was supported by ILL within the framework of Proposal No. 9-13-778 and the joint Campus France Amadee 42224PD / OEAD WTZ FR 10/2019 project.

This work benefited from the use of the SasView application, originally developed under NSF award DMR-0520547. SasView contains code development with funding from the European Union's Horizon 2020 research and innovation programme under the SINE2020 project, grant agreement No 654000.

We thank Prof. Erik Reimhult from the University of Natural Resources and Life Sciences Vienna and the HSRM project NANOBILD for access to SEM.

We acknowledge the Partnership for Soft and Condensed matter (PSCM) for access to the ESRF and ILL facilities and Pierre Lloria for support with the instruments. We thank Sylvain Prevost and Ralf Schweins for support with SANS experiments and data reduction. We want to acknowledge Mauricio Alvarez for his efforts with rheology experiments. We thank Prof. C. V. Stevens (Dpt. Green Chemistry and Technology, Ghent University, Ghent, Belgium) for providing us access to the hydrogenation facility.

### Associated Content

The following files are available free of charge: SDS-PAGE gels of SF, ATR-FTIR spectra of pure lipids, SANS fitting approach to SL-C18:0 and calculation of scattering length densities, contrast matching data for SF-SL-C18:1, absorption measurements for SF-SL-C18:0 and photographs of all gels.

### Author Information

#### Corresponding Authors

\*Andrea Lassenberger

Institut Laue-Langevin, 71 Avenue des Martyrs, 38042 Grenoble, France

<https://orcid.org/0000-0002-7922-4853>

[lassenberger@ill.fr](mailto:lassenberger@ill.fr) †

\*Niki Baccile

Sorbonne Université, Centre National de la Recherche Scientifique, Laboratoire de Chimie de la Matière Condensée de Paris, LCMCP, F-75005 Paris, France

[niki.baccile@sorbonne-universite.fr](mailto:niki.baccile@sorbonne-universite.fr)

<https://orcid.org/0000-0003-3142-3228>

### Author Contributions

AL has planned the project, designed and conducted the experiments and written the manuscript. NB has conducted experiments and reviewed the manuscript. AM was local contact for SANS experiment and reviewed the manuscript, LP helped with data fitting and reviewing. All authors have given approval to the final version of the manuscript.

### Literature

1. L.-D. Koh, Y. Cheng, C.-P. Teng, Y.-W. Khin, X.-J. Loh, S.-Y. Tee, M. Low, E. Ye, H.-D. Yu, Y.-W. Zhang, M.-Y. Han, *Prog. Polym. Sci.*, 2015, **46**, 86-110.
2. A. S. Gobin, V. E. Froude, A. B. Mathur, *J. Biomed. Mater. Res., Part A*, 2005, **74A**, 465-473.
3. R. Liu, Q. Deng, Z. Yang, D. Yang, M.-Y. Han, X. Y. Liu, *Adv. Funct. Mater.*, 2016, **26**, 5534-5541.
4. U.-J. Kim, J. Park, H. Joo Kim, M. Wada, D. L. Kaplan, *Biomaterials*, 2005, **26**, 2775-2785.
5. A. R. Murphy, D. L. Kaplan, *J. Mater. Chem.*, 2009, **19**, 6443-6450.
6. H. Yamada, H. Nakao, Y. Takasu, K. Tsubouchi, *Mater. Sci. Eng. C*, 2001, **14**, 41-46.
7. D. N. Rockwood, R. C. Preda, T. Yücel, X. Wang, M. L. Lovett, D. L. Kaplan, *Nat. Protoc.*, 2011, **6**, 6012-6031.
8. A. P. Tabatabai, K. M. Weigandt, D. L. Blair, *Phys. Rev. E*, 2017, **96**, 022405.
9. N. Kasoju, U. Bora, *Adv. Healthcare Mater.*, 2012, **1**, 393-412.
10. Y. Kishimoto, H. Morikawa, S. Yamanaka, Y. Tamada, *Mater. Sci. Eng. C*, 2017, **73**, 498-506.
11. H. Tao, B. Marelli, M. Yang, B. An, M. S. Onses, J. A. Rogers, D. L. Kaplan, F. G. Omenetto, *Adv. Mater.*, 2015, **27**, 4273-4279.
12. X. Chen, Z. Shao, N. S. Marinkovic, L. M. Miller, P. Zhou, M. R. Chance, *Biophys. Chem.*, 2001, **89**, 25-34.
13. U.-J. Kim, J. Park, C. Li, H.-J. Jin, R. Valluzzi, D. L. Kaplan, *Biomacromolecules*, 2004, **5**, 786-792.
14. A. Martel, M. Burghammer, R. Davies, E. DiCola, P. Panine, J.-B. Salmon, C. Riekkel, *Biomicrofluidics*, 2008, **2**, 024104.
15. X.-H. Zong, P. Zhou, Z.-Z. Shao, S.-M. Chen, X. Chen, B.-W. Hu, F. Deng, W.-H. Yao, *Biochemistry*, 2004, **43**, 11932-11941.
16. X. Hu, K. Shmelev, L. Sun, E.-S. Gil, S.-H. Park, P. Cebe, D. L. Kaplan, *Biomacromolecules*, 2011, **12**, 1686-1696.
17. M. Boulet-Audet, A. E. Terry, F. Vollrath, C. Holland, *Acta Biomater.*, 2014, **10**, 776-784.
18. P. R. Laity, C. Holland, *Int. J. Mol. Sci.*, 2016, **17**, 1812.
19. X. Wang, J. Kluge, G. G. Leisk, D. L. Kaplan, *Biomaterials*, 2008, **29**, 1054-1064.
20. M. Floren, C. Migliaresi, A. Motta, *J. Funct. Biomater.*, 2016, **7**, 26.
21. X. Wu, J. Hou, M. Li, J. Wang, D. L. Kaplan, S. Lu, *Acta Biomater.*, 2012, **8**, 2185-2192.
22. J. H. Park, M. H. Kim, L. Jeong, D. Cho, O. H. Kwon, W. H. Park, *J. Sol-Gel Sci. Technol.*, 2014, **71**, 364-371.

23. Z. H. Ayub, M. Arai, K. Hirabayashi, *Biosci., Biotechn. Biochem.*, 1993, **57**, 1910-1912.
24. A. Matsumoto, J. Chen, A. L. Collette, U.-J. Kim, G. H. Altman, P. Cebe, D. L. Kaplan, *J. Phys. Chem. B*, 2006, **10**, 21630-21638.
25. N. Kasoju, N. Hawkins, O. Pop-Georgievski, D. Kubies, F. Vollrath, *Biomater. Sci.*, 2016, **4**, 460-473.
26. K. Numata, T. Katashima, T. Sakai, *Biomacromolecules*, 2011, **12**, 2137-2144.
27. P. Dubey, L. Nawale, D. Sarkar, A. Nisal, A. Prabhune, *RSC Adv.*, 2015, **5**, 33955-33962.
28. P. Dubey, S.Kumar, V. K. Aswal, S. Ravindranathan, P. R. Rajamohanan, A. Prabhune, A. Nisal, *Biomacromolecules*, 2016, **17**, 3318-3327.
29. S. L. Fu, S. R. Wallner, W. B. Bowne, M. D. Hagler, M. E. Zenilman, R. Gross, M. H. Bluth, *J. Surg. Res.*, 2008, **148**, 77-82.
30. J. N. Sleiman, S. A. Kohlhoff, P. M. Roblin, S. Wallner, R. Gross, M. R. Hammerschlag, M. E. Zenilman, M. H. Bluth, *Ann. Clin. Lab. Sci.*, 2009, **39**, 60-63.
31. G. Ben Messaoud, P. Le Griel, D. Hermida-Merino, S. L. K. W. Roelants, W. Soetaert, C. V. Stevens, N. Baccile, *Chem. Mater.*, 2019, **31**, 4817-4830.
32. Y. Zheng, M. K. Liong Han, Q. Jiang, B. Li, J. Feng, A. del Campo, *Mater. Horiz.*, 2020, **7**, 111-116.
33. C. A. DeForest, K. S. Anseth, *Nat. Chem.*, 2011, **3**, 925-931.
34. S. Das, U. Subuddhi, *J. Pharm. Anal.*, 2019, **9**, 108-116.
35. P. M. Kharkar, K. L. Kiick, A. M. Kloxin, *Chem. Soc. Rev.*, 2013, **42**, 7335-7372.
36. A. Martel, M. Burghammer, R. J. Davies, E. Di Cola, C. Vendrely, C. Riekel, *J. Am. Chem. Soc.*, 2008, **130**, 17070-17074.
37. S. Nagarkar, T. Nicolai, C. Chassenieux, A. Lele, *Phys. Chem. Chem. Phys.*, 2010, **12**, 3834-3844.
38. A.-S. Cuvier, J. Berton, C. V. Stevens, G. C. Fadda, F. Babonneau, I. N. A. Van Bogaert, W. Soetaert, G. Pehau-  
Arnaudet, N. Baccile, *Soft Matter*, 2014, **10**, 3950-3959.
39. S. Manet, A.-S. Cuvier, C. Valotteau, G. C. Fadda, J. Perez, E. Karakas, S. Abel, N. Baccile, *J. Phys. Chem. B*,  
2015, **119**, 13113-13133.
40. <https://www.ill.eu/fr/users/support-labs-infrastructure/software-scientific-tools/grasp/>. (10/2020)
41. 10.5291/ILL-DATA.9-13-778.
42. <http://www.sasview.org>. (11/2020)
43. <https://www.nist.gov/ncnr/data-reduction-analysis/sans-software>. (02/2020)
44. P. Dubey, S. Kumar, S. Ravindranathan, S. Vasudevan, V. K. Aswal, P. R. Rajamohanan, A. Nisal, A. Prabhune,  
*Mater. Chem. Phys.*, 2018, **203**, 9-16.
45. B. Hammouda, *J. Appl. Crystallogr.*, 2010, **43**, 716-719.
46. M. Kotlarchyk, S. H. Chen, *J. Chem. Phys.*, 1983, **79**, 2461-2469.
47. S. Manet, A.-S. Cuvier, C. Valotteau, G. C. Fadda, J. Perez, E. Karakas, S. Abel, N. Baccile, *J. Phys. Chem. B*,  
2015, **119**, 13113-13133.
48. P. Dhasaiyan, P. Le Griel, S. Roelants, E. Redant, I. N. A. Van Bogaert, S. Prevost, B. L. V Prasad, N. Baccile,  
*Chem. Phys. Chem.*, 2017, **18**, 643-652.
49. A. Rüter, S. Kuczera, D. J. Pochan, U. Olsson, *Langmuir*, 2019, **35**, 5802-5808.
50. L. A. Feigin, D. I. Svergun, *Structure Analysis by Small-Angle X-ray and Neutron Scattering*, John Wiley & Sons,  
Ltd., New Jersey, 1989.
51. N. Chantong, S. Damrongsakkul, J. Ratanavaraporn, *J. Surfactants Deterg.*, 2019, **22**, 1395-1407.
52. X. Hu, D. Kaplan, P. Cebe, *Macromolecules*, 2008, **41**, 3939-3948.
53. J. Kong, S. Yu, *Acta Biochim. Biophys. Sin.*, 2007, **39**, 549-559.

54. X. Hu, D. Kaplan, P. Cebe, *Macromolecules*, 2006, **39**, 6161-6170.
55. A. Barth, C. Zscherp, *Q. Rev. Biophys.*, 2002, **35**, 369-430.
56. S. Cai, B. R. Singh, *Biochemistry*, 2004, **43**, 2541-2549.
57. I. Greving, C. Dicko, A. Terry, P. Callow, F. Vollrath, *Soft Matter*, 2010, **6**, 4389-4395.
58. I. Roy, M. N. Gupta, *Biotechnol. Appl. Biochem.*, 2004, **39**, 165-177.
59. G. B. Strambini, E. Gabellieri, *Biophys. J.*, 1996, **70**, 971-976.
60. M. Boulet-Audet, F. Vollrath, C. Holland, *J. Exp. Biol.*, 2015, **218**, 3138-3149.
61. K. Steck, S. Dieterich, C. Stubenrauch, F. Giesselmann, *J. Mater. Chem. C*, 2020, **8**, 5335-5348.
62. J. Teixeira, *J. Appl. Crystallogr.*, 1988, **21**, 781-785.
63. T. Puspitasari, K. M. L. Raja, D. S. Pangerteni, A. Patriati, E. G. R. Putra, *Proc. Chem.*, 2012, **4**, 186-193.
64. M. Yao, D. Su, W. Wang, X. Chen, Z. Shao, *ACS Appl. Mater. Interfaces*, 2018, **10**, 38466-38475.
65. J. L. Whittaker, R. Balu, R. Knott, L. de Campo, J. P. Mata, C. Rehm, A. J. Hill, N. K. Dutta, N. Roy Choudhury, *Int. J. Biol. Macromol.*, 2018, **114**, 998-1007.
66. L. F. Drummy, B. L. Farmer, R. R. Naik, *Soft Matter*, 2007, **3**, 877-882.
67. Y. Cheng, L.-D. Koh, D. Li, B. Ji, M.-Y. Han, Y.-W. Zhang, *J. R. Soc. Interface*, 2014, **11**, 20140305-20140305.
68. J. Ming, B. Zuo, *J. Appl. Polymer Sci.*, 2012, **125**, 2148-2154.
69. Z. Gong, L. Huang, Y. Yang, X. Chen, Z. Shao, *Chem. Comm.*, 2009, **48**, 7506-7508.
70. S. Ling, W. Chen, Y. Fan, K. Zheng, K. Jin, H. Yu, M. J. Buehler, D. L. Kaplan, *Prog. Polym. Sci.*, 2018, **85**, 1-56.
71. P. Georgiades, E. di Cola, R. K. Heenan, P. D. A. Pudney, D. J. Thornton, T. A. Waigh, *Biopolymers*, 2014, **101**, 1154-1164.
72. M. Shibayama, *Polym. J.*, 2011, **43**, 18-34.
73. O. Glatter, O. Kratky, *Small angle x-ray scattering*, Academic Press Inc. Ltd., London 1982.
74. M. A. Jamros, L. C. Oliveira, P. C. Whitford, J. N. Onuchic, J. A. Adams, P. A. Jennings, *PLOS Comput. Biol.*, 2012, **8**, e1002695.
75. T. Ando, S. Yamanaka, S. Kohjiya, K. Kajiwara, *Polym. Gels Networks*, 1993, **1**, 45-60.
76. H.-X. Zhou, X. Pang, *Chem. Rev.*, 2018, **118**, 1691-1741.
77. C.-Z. Zhou, F. Confalonieri, M. Jacquet, R. Perasso, Z.-G. Li, J. Janin, *Proteins: Struct., Funct. Bioinf.*, 2001, **44**, 119-122.
78. D. E. Otzen, *Curr. Protein Pept. Sci.*, 2010, **11**, 355-71.
79. Z. Najarzadeh, J. N. Pedersen, G. Christiansen, S. A. Shojaosadati, J. S. Pedersen, D. E. Otzen, *Biochim. Biophys. Acta - Proteins Proteomics*, 2019, **1867**, 140263.
80. D. Jayawardane, F. Pan, J. R. Lu, X. Zhao, *Langmuir*, 2016, **32**, 8202-8211.
81. P. Ball, J. E. Hallsworth, *Phys. Chem. Chem. Phys.*, 2015, **17**, 8297-8305.
82. M. Davidovic, C. Mattea, J. Qvist, B. Halle, *J. Am. Chem. Soc.*, 2009, **131**, 1025-1036.
83. P. Lo Nostro, B. W. Ninham, *Chem. Rev.*, 2012, **112**, 2286-2322.
84. N. Baccile, A.-S. Cuvier, S. Prévost, C. V. Stevens, E. Delbeke, J. Berton, W. Soetaert, I. N. A. Van Bogaert, S. Roelants, *Langmuir*, 2016, **32**, 10881-10894.
85. M. Masuda, T. Shimizu, *Langmuir*, 2004, **20**, 5969-5977.
86. S. Hirlekar, D. Ray, V. K. Aswal, A. A. Prabhune, A. Nisal, *ACS Omega*, 2020, **5**, 28571-28578.
87. J. Zhu, Y. Zhang, H. Shao, X. Hu, *Polymer*, 2008, **49**, 2880-2885.
88. A. Nisal, C. Kalelkar, J. Bellare, A. Lele, *Rheol. Acta.*, 2013, **52**, 833-840.
89. A. Matsumoto, A. Lindsay, B. Abedian, D.L. Kaplan, *Macromol. Biosci.*, 2008, **8**, 1006-1018.



## Supporting Information

### Interpenetrated biosurfactant–silk fibroin networks - A SANS study

Andrea Lassenberger,<sup>\*,1</sup> Anne Martel,<sup>1</sup> Lionel Porcar,<sup>1</sup> Niki Baccile<sup>\*,2</sup>

<sup>1</sup>Institut Laue-Langevin, 71 Avenue des Martyrs, 38042 Grenoble Cedex 9, France

<sup>2</sup>Centre National de la Recherche Scientifique, Laboratoire de Chimie de la Matière Condensée de Paris, LCMCP, Sorbonne Université, Paris F-75005, France

#### Contents

1. SDS-PAGE of regenerated silk fibroin (SF) .....	1
2. SANS fitting approach .....	2
3. Calculation of neutron scattering length densities. ....	3
4. SANS models.....	3
5. Inverse approach: subtracting SF from the composite signal (SANS) .....	5
6. Contrast matching experiments .....	6
7. References.....	8



1. SDS-PAGE of regenerated silk fibroin (SF)

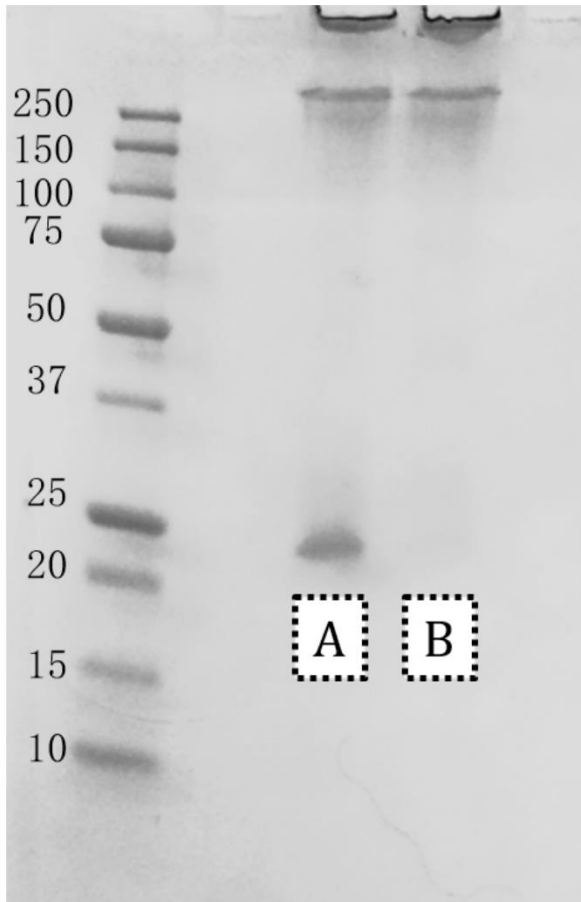


**Figure S 1.** SDS-PAGE of SF solution after dialysis in H<sub>2</sub>O. Band **A**) The disulfide bond between the light chain (FibL) and the heavy chain (FibH) was cleaved with  $\beta$ -mercaptoethanol, resulting in two distinct bands at >250 kDa (FibH) and ~25 kDa (FibL). Band **B**) SF without treatment of  $\beta$ -mercaptoethanol resulting in a single band >250 kDa.

## 2. SANS fitting approach

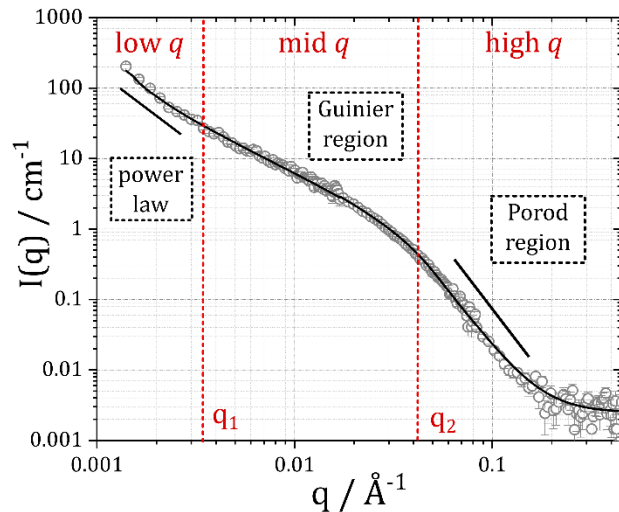


**Figure S 2** Representative SF neutron scattering pattern with  $q$ -regions discussed in the main manuscript. The characteristic length scales  $q_1$  and  $q_2$ , described in equation 2 in the main text are illustrated in red with  $q_1 \approx 0.0035 \text{ \AA}^{-1}$  and  $q_2 \approx 0.04 \text{ \AA}^{-1}$ .

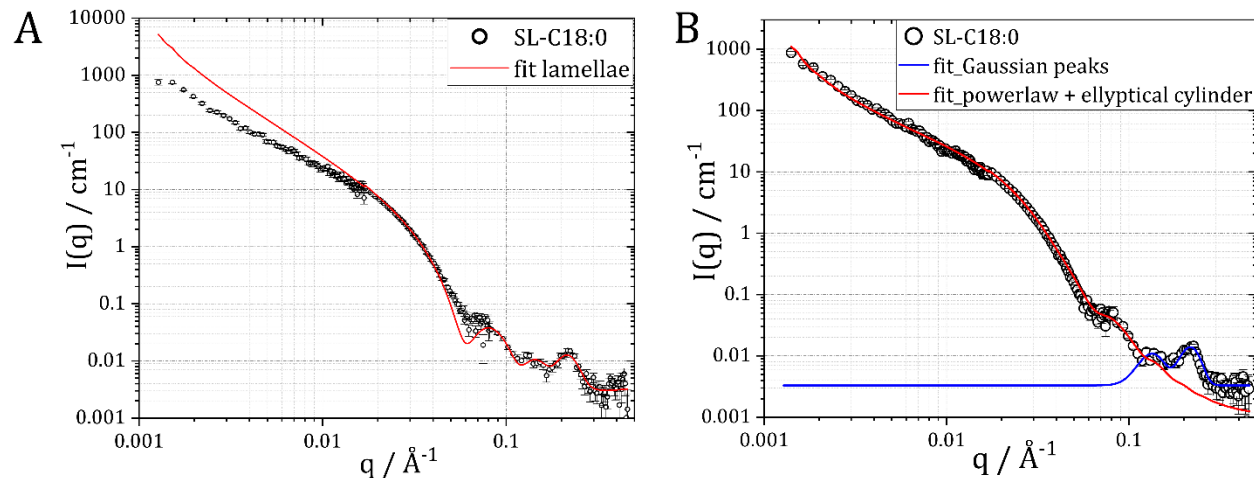


**Figure S 3.** SANS fitting approaches for SL-C18:0. **A)** Approach with a model for a lamellar phase. **B)** Model combination of a power law + elliptical cylinder (red) and two Gaussian peaks (blue). It is noteworthy the first Gauss peak coincides with the second oscillation of the elliptical cylinder form factor whereas the third peak known to be the repeating inter-lipid distance in the twisted ribbons formed by SL-C18:0<sup>1</sup>. Open symbols represent the experimental data, continuous lines the fits.

### 3. Calculation of neutron scattering length densities.

The *SLD* of sophorolipids was calculated with SasView as *SLD (SL)<sub>head</sub>* being the *SLD* of the hydrophilic sugar headgroups and *SLD (SL)<sub>tail</sub>* as the *SLD* of the hydrophobic saturated (SL-C18:0) or mono-unsaturated (SL-C18:1) oleic or stearic acid derived tail. H-D exchange was taken into account. The different head and tail *SLDs* were only taken into account for SL-C18:1. For the fitting of SL-C18:0 we considered only *SLD (SL)<sub>tail</sub>* for simplicity. The *SLD* of SF was calculated with the biomolecular *SLD* calculator available on the ISIS homepage<sup>2</sup> by using the amino acid sequence provided from UniProt<sup>3</sup> and an estimated H-D exchange of 90 %:

$$\text{SL-C18:1 (in D}_2\text{O): } SLD (SL)_{\text{head}} = 2.88 \cdot 10^{-6} \text{ \AA}^{-2}, SLD (SL)_{\text{tail}} = 0.25 \cdot 10^{-6} \text{ \AA}^{-2},$$

$$\text{SL-C18:0 (in 100 \% D}_2\text{O): } SLD (SL)_{\text{tail}} = 0.19 \cdot 10^{-6} \text{ \AA}^{-2}, \text{ in 51 \% D}_2\text{O: } SLD (SL)_{\text{tail}} = 0.1 \cdot 10^{-6} \text{ \AA}^{-2}$$

$$SLD (SF)_{\text{D}_2\text{O}} = 3.66 \cdot 10^{-6} \text{ \AA}^{-2}, SLD (SF)_{\text{H}_2\text{O}} = 2.3 \cdot 10^{-6} \text{ \AA}^{-2},$$

$$SLD_{\text{D}_2\text{O}} = 6.3 \cdot 10^{-6} \text{ \AA}^{-2}, SLD_{\text{H}_2\text{O}} = -0.56 \cdot 10^{-6} \text{ \AA}^{-2}$$

### 4. SANS models

Samples were fitted with the following model combinations:

SL-C18:1 – core-shell ellipsoid<sup>4</sup>

SL-C18:0 – power law + elliptical cylinder<sup>5</sup> + 2 Gaussian peaks

SF gelled (D<sub>2</sub>O) – power law + Guinier-Porod

SF-SL-C18:1 - power law + Guinier-Porod + core-shell ellipsoid

SF-SL-C18:0 - power law + Guinier-Porod + power law + elliptical cylinder + 2 Gaussian peaks

The volume fractions  $\Phi$  ('scale') were held constant throughout the whole fitting process

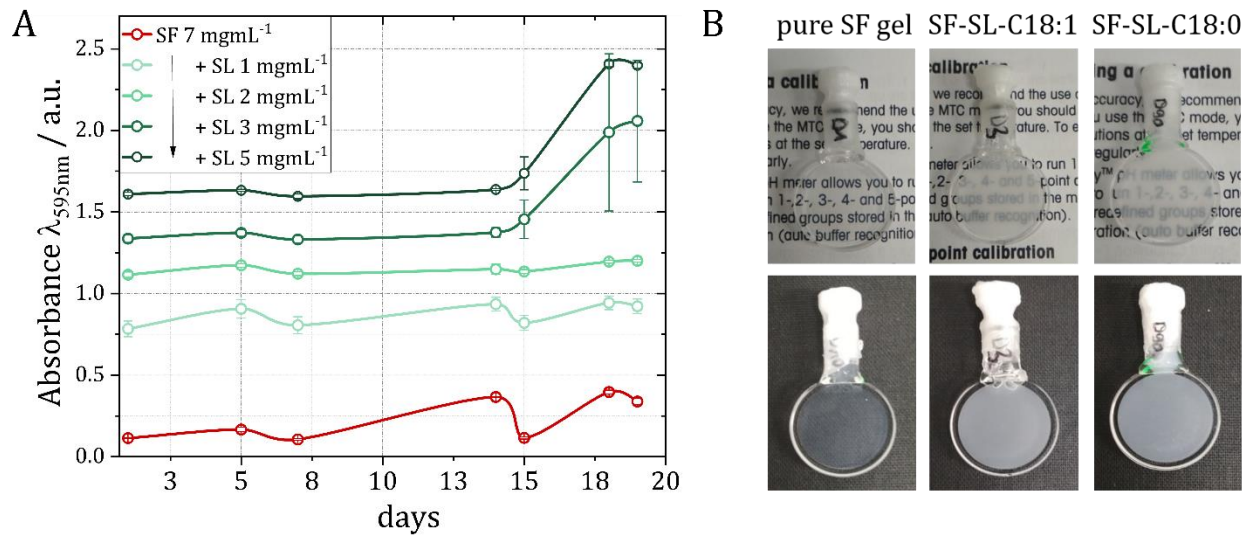


**Figure S 4. A)** Absorption measurements at 595 nm for SF at 7 mgmL<sup>-1</sup> and SF-SL-C18:0 composite gels at the indicated lipid concentrations. Results are presented for completeness but not used for interpretation. **B)** Photographs of SF gels and composite gels in D<sub>2</sub>O in the SANS measurement cells, showing that all gels are homogenous.

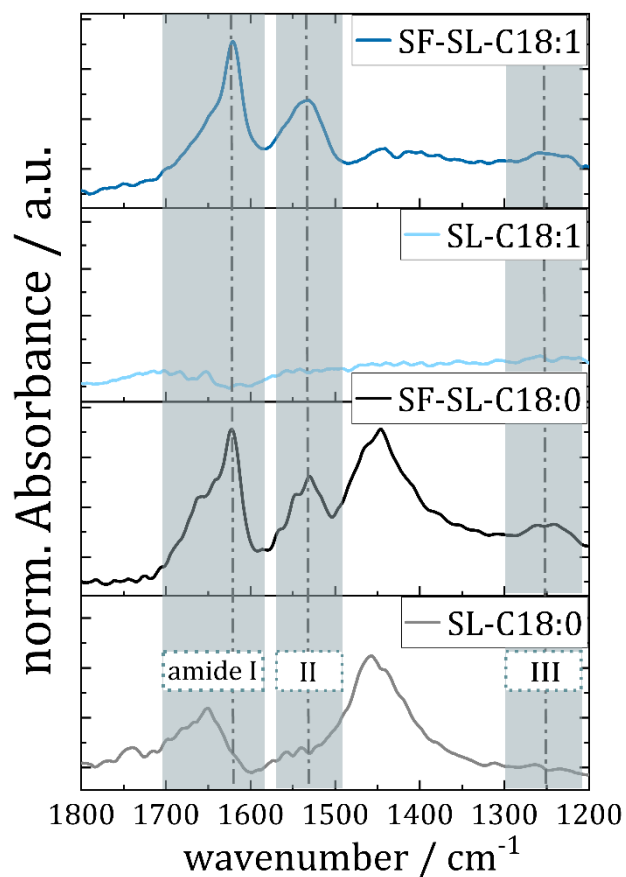


**Figure S 5.** ATR-FTIR spectra of composite gels and the respective lipids in H<sub>2</sub>O from top to bottom: SF-SL-C18:1 composite, SL-C18:1 at 5 mgmL<sup>-1</sup>, SF-SL-C18:0 composite and SL-C18:0 lipid at 5 mgmL<sup>-1</sup>. Spectra were normalized to the maximum absorption in the amide I band at 1696 cm<sup>-1</sup>. The amide I, II and III regions are highlighted to show that there is no interference of the lipid bands with the peaks discussed in the main manuscript for determination of secondary structure. Note that at such small concentrations and measurement in H<sub>2</sub>O the COOH band of SL at 1704 cm<sup>-1</sup> is absent. The broad peak between 1400 and 1500 cm<sup>-1</sup> in the SL-C18:0 spectrum can be assigned to scissoring ( $\delta$ ) of CH<sub>2</sub> and stretching ( $\nu$ ) of CO and CC groups in the carbohydrate part of SL and the  $\nu_s$  of COO<sup>-</sup>. The peak is absent in SL-C18:1 since an ATR geometry was used. SL-C18:0 is a gel with solid assemblies that adsorbs to the crystal, resulting in much higher absorption than SL-C18:0, which is liquid.

## 5. Inverse approach: subtracting SF from the composite signal (SANS)

To further support our hypothesis that the structure of the employed lipids is intact, in particular that of SL-C18:1 for which contrast matching experiments were less striking than for SL-C18:0, we subtracted the scattering intensity of pure SF from that of the composite gels and compared it with that of the pure lipids. Figure S6A displays the resulting curve  $I(q)_{SF-SL-C18:1} - I(q)_{SF}$  (grey) and Figure 6B shows  $I(q)_{SF-SL-C18:0} - I(q)_{SF}$ , plotted together with the respective pure lipid. In Figure S6A (grey) the signal of the pure lipid is recovered at  $q > 0.025 \text{ \AA}^{-1}$  and fitted with the same core-shell ellipsoid model as pure SL-C18:1, letting the values for core, shell and axis ratio and background vary. The fitted parameters (Table S1) are very close to that of the pure lipid, supporting our hypothesis that the structure of SL-C18:1 micelles does not change in presence of SF. The difference in scattering intensity at  $q < 0.025 \text{ \AA}^{-1}$  stems from the change in shape of SF

and the increased network inhomogeneities as is described in the main manuscript. One could argue that the change in signal intensity at low  $q$  stems from a change in shape of SL-C18:1. This however could be ruled out with contrast matching experiments (see section 5) where SF is matched with the resulting signal being flat at low  $q$ .

In Figure S6B the signal  $I(q)_{SF-SL-C18:0} - I(q)_{SF}$  is fitted with the same combined power law – elliptical cylinder – gauss peak model as pure SL-C18:0 by varying the values for cylinder diameter, axis ratio and background (Table S1). The resulting difference is much less pronounced and the signal of the pure lipid is almost completely recovered, which is in line with contrast matching experiments for this system.

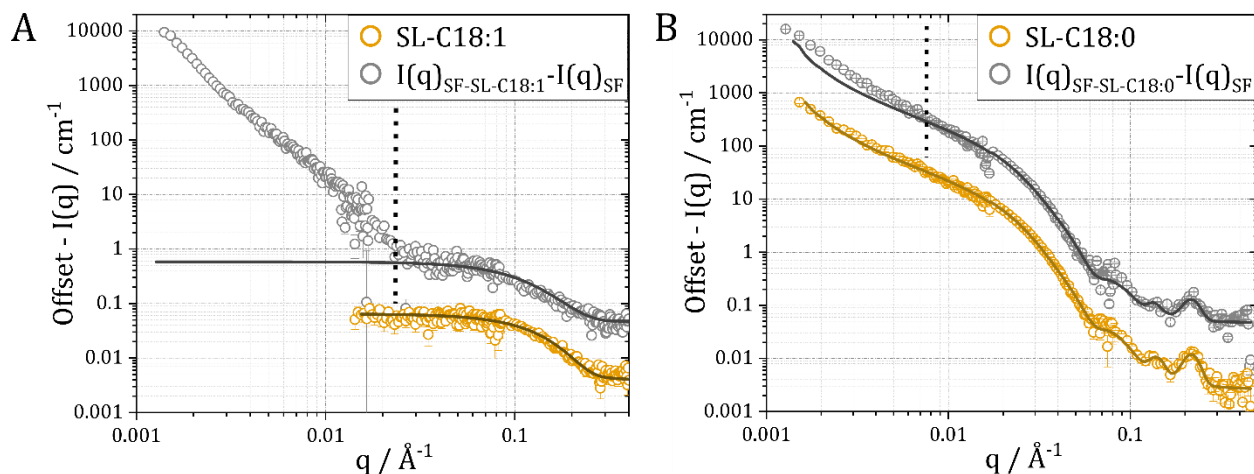


**Figure S 6.** Neutron scattering data of hydrogels four weeks after dialysis and lipids, all in  $D_2O$  with SF at  $7 \text{ mgmL}^{-1}$  and SL at  $5 \text{ mgmL}^{-1}$ . The signal of SF gelled is subtracted from the signal of the composite gels yielding the curves **A**)  $I(q)_{SF-SL-C18:1} - I(q)_{SF}$  (grey), plotted together with  $I(q)$  of pure SL-C18:1 and **B**)  $I(q)_{SF-SL-C18:0} - I(q)_{SF}$  (grey), displayed with the signal for pure SL-C18:0. The grey curves are fitted with the same models and similar parameters (cf. Table S1) as the pure lipids. The vertical lines mark where the model deviates significantly from the data. Above this  $q$  value the signal of the respective lipid is fully recovered whereas below it, the resulting signal intensity stems from changes in the overall network structure.

## 6. Contrast matching experiments

SF-SL-C18:1 was attempted to be measured under contrast matching conditions (Figure S7). We aimed to measure at 51 %  $D_2O$ , which is the match point of SF, to gain information about the integrity of SL-C18:1 micelles. However, the scattering intensity of SL-C18:1 is already quite low in  $D_2O$  at the chosen concentration and the signal was lost almost completely in the incoherent background at 51 %  $D_2O$ , also for the pure lipid (Figure S7, yellow). The only information that we can extract from this is, that the SL-C18:1 micelles did not form e.g. worm-like micelles or other aggregates in presence of SF as this would result in an increase of scattering intensity at low  $q$ , visible at contrast matching conditions.<sup>6</sup>

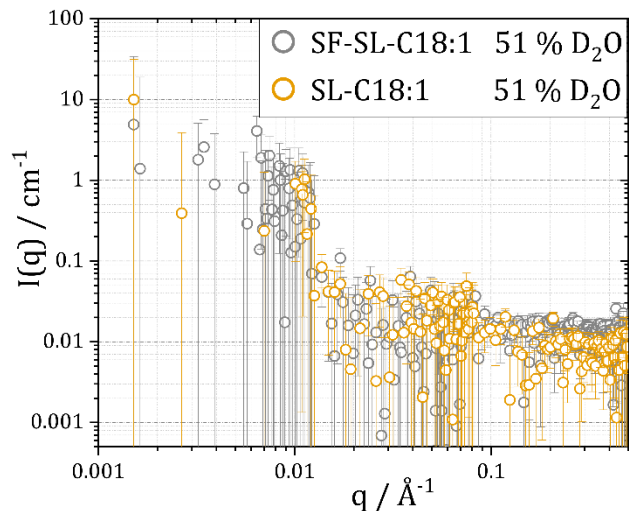


**Figure S 7.** SANS data for SF-SL-C18:1 composite gel (grey) and pure SL-C18:1 (yellow) at the match point of SF (51 % D<sub>2</sub>O). The signal of SL is lost in high incoherent scattering background stemming from 49 % H<sub>2</sub>O. At low  $q$  only very diffuse scattering intensity is observed, supporting the hypothesis that the scattering difference observed in Figure S6A stems only from a change in network structure. If SL-C18:1 would have formed e.g. wormlike micelles, it would be visible under contrast matching conditions in an increase of  $I(q)$  at low  $q$ .

In addition to the discussed contrast matching experiments, we have considered to perform measurements at the match point of the sophorolipids. This is however not straight forward since the head- and tail of SL have two very different match points, whereas the match point for the sophorose headgroup is very close to that of SF (49 % D<sub>2</sub>O vs. 51 % D<sub>2</sub>O for SF). The match point of the aliphatic tail is at 8 % D<sub>2</sub>O, which causes a high incoherent background. We opted thus for matching SF.

**Table S 1.** Fitted parameters for sophorolipids in pure micellar (SL-C18:1) and ribbon containing form (SL-C18:0) and in the composite hydrogels. Values for lipids in the composite gels were obtained by feeding the fitted parameters for SF (*cf.* Table 1 in the main text) into the model for the composite and then allowing the parameters for radius and axis ratio for SL to vary. Alternatively, the signal of SF was subtracted from that of the composite and the resulting signal was fitted with a core-shell ellipsoid model (SL-C18:1) or a combination of power law-elliptical cylinder-gauss peak (SL-C18:0).

	solvent /%D <sub>2</sub> O	SLD / x10 <sup>-6</sup> Å <sup>-2</sup>		radius <sub>min</sub> / Å	radius <sub>maj</sub> / Å	t <sub>shell</sub> / Å	peakpos / Å <sup>-1</sup>
		tail	head				
SL-C18:1	100	0.3	2.88	5 ± 0.1	20 ± 0.3	9 ± 0.9	-
SL-C18:1 in comp gel (I(q) <sub>SF-SL-C18:1</sub> -I(q) <sub>SL-C18:1</sub> )	100	0.3	2.88	5 ± 0.3	24 ± 0.4	7 ± 1.0	-
SL-C18:1 in comp gel (I(q) <sub>SF-SL-C18:1</sub> -I(q) <sub>SF</sub> )	100	0.3	2.88	5 ± 0.3	23 ± 0.5	8 ± 0.2	-
SL-C18:0	100	0.19	-	53 ± 0.2	122 ± 0.5	-	0.217
SL-C18:0 in comp gel (I(q) <sub>SF-SL-C18:0</sub> -I(q) <sub>SL-C18:0</sub> )	100	0.19	-	49 ± 0.1	122 ± 0.5	-	0.217
SL-C18:0 in comp gel (I(q) <sub>SF-SL-C18:0</sub> -I(q) <sub>SF</sub> )	100			55 ± 0.2	122 ± 0.4	-	0.217

SL-C18:0	51	0.1	-	53 ±0.3	116 ± 0.5	-	-
SL-C18:0 in comp. gel	51	0.1	-	55 ±0.2	119±0.6	-	-

## 7. References

1. A.-S.Cuvier, J. Berton, C. V. Stevens, G. C. Fadda, F. Babonneau, I. N. A. Van Bogaert, W. Soetaert, G. Pehau-  
Arnaudet and N. Baccile, *Soft Matter*, **2014**, 10, 3950-3959.
2. <http://pslhc.isis.rl.ac.uk/Pslhc/>.
3. <https://www.uniprot.org>.
4. M. Kotlarchyk and S. H. Chen, *J. Chem. Phys.*, **1983**, 79, 2461-2469.
5. L. A. Feigin, and D. I. Svergun, *Structure analysis by small-angle X-ray and neutron scattering*. Plenum Press,  
New York, 1989.
6. P. Malo de Molina and M. Gradzielski, *Gels*, **2017**, 3 , 1-30.